

# 1 Seasonal study of stable carbon and nitrogen isotopic composition 2 in fine aerosols at a Central European rural background station

3  
4 Petr Vodička<sup>1,2</sup>, Kimitaka Kawamura<sup>1</sup>, Jaroslav Schwarz<sup>2</sup>, Bhagawati Kunwar<sup>1</sup>, Vladimír  
5 Ždímal<sup>2</sup>

6  
7 <sup>1</sup> Chubu Institute for Advanced Studies, Chubu University, 1200 Matsumoto-cho, Kasugai 487–8501, Japan

8 <sup>2</sup>Institute of Chemical Process Fundamentals of the Czech Academy of Science, Rozvojová 2/135, 165 02, Prague  
9 6, Czech Republic

10 *Correspondence to:* vodicka@icpf.cas.cz (P. Vodička), kkawamura@isc.chubu.ac.jp (K. Kawamura)

11  
12 **Abstract.** A study of the stable carbon isotope ratios ( $\delta^{13}\text{C}$ ) of total carbon (TC) and the nitrogen  
13 isotope ratios ( $\delta^{15}\text{N}$ ) of total nitrogen (TN) was carried out for fine aerosol particles (PM<sub>1</sub>) collected  
14 every two days with a 24 h sampling period at a rural background site in Košetice (Central Europe)  
15 from September 27, 2013, to August 9, 2014 (n=146). We found a seasonal pattern for both  $\delta^{13}\text{C}$  and  
16  $\delta^{15}\text{N}$ . The seasonal variation in  $\delta^{15}\text{N}$  was characterized by lower values (av.  $13.1\pm 4.5\%$ ) in winter and  
17 higher values ( $25.0\pm 1.6\%$ ) in summer. Autumn and spring were transition periods when the isotopic  
18 composition gradually changed due to the changing sources and the ambient temperature. The seasonal  
19 variation in  $\delta^{13}\text{C}$  was less pronounced but more depleted in  $^{13}\text{C}$  in summer ( $-27.8\pm 0.4\%$ ) as compared  
20 to winter ( $-26.7\pm 0.5\%$ ).

21 A comparative analysis with water-soluble ions, organic carbon, elemental carbon, trace gases and  
22 meteorological parameters (mainly ambient temperature) has shown major associations with the  
23 isotopic compositions, which enlightened the corresponding processes. A comparison of  $\delta^{15}\text{N}$  with  $\text{NO}_3^-$ ,  
24  $\text{NH}_4^+$  and organic nitrogen (OrgN) revealed that although a higher content of  $\text{NO}_3^-$  was associated with  
25 a decrease in the  $\delta^{15}\text{N}$  of TN,  $\text{NH}_4^+$  and OrgN caused increases. The highest concentrations of nitrate,  
26 mainly represented by  $\text{NH}_4\text{NO}_3$ , related to the emissions from biomass burning, leading to an average  
27  $\delta^{15}\text{N}$  of TN (13.3%) in winter. During spring, the percentage of  $\text{NO}_3^-$  in PM<sub>1</sub> decreased. An enrichment  
28 of  $^{15}\text{N}$  was probably driven by the equilibrium exchange between the gas and aerosol phases ( $\text{NH}_3(\text{g})$   
29  $\leftrightarrow \text{NH}_4^+(\text{p})$ ), which is supported by the increased ambient temperature. This equilibrium was suppressed  
30 in early summer when the molar ratios of  $\text{NH}_4^+/\text{SO}_4^{2-}$  reached 2, and the nitrate partitioning in aerosol  
31 was negligible due to the increased ambient temperature. Summertime  $\delta^{15}\text{N}$  values were among the  
32 highest, suggesting the aging of ammonium sulfate and OrgN aerosols. Such aged aerosols can be  
33 coated by organics in which  $^{13}\text{C}$  enrichment takes place by the photooxidation process. This result was  
34 supported by a positive correlation of  $\delta^{13}\text{C}$  with ambient temperature and ozone, as observed in the  
35 summer season.

36 During winter, we observed an event with the lowest  $\delta^{15}\text{N}$  and highest  $\delta^{13}\text{C}$  values. The winter *Event*  
37 occurred in prevailing southeast air masses. Although the higher  $\delta^{13}\text{C}$  values probably originated from  
38 biomass burning particles, the lowest  $\delta^{15}\text{N}$  values were probably associated with agriculture emissions  
39 of  $\text{NH}_3$  under low temperature conditions ( $< 0^\circ\text{C}$ ).  
40

## 41 **1. Introduction**

42  
43 Aerosols have a strong impact on key processes in the atmosphere associated with climate change, air  
44 quality, rain patterns and visibility (Fuzzi et al., 2015; Hyslop, 2009). Because these processes are still  
45 insufficiently understood, they are studied intensively. One approach to explore chemical processes  
46 taking place in atmospheric aerosols is the application of stable carbon ( $\delta^{13}\text{C}$ ) and nitrogen ( $\delta^{15}\text{N}$ )  
47 isotope ratios. These isotopes can provide unique insight on source emissions along with physical and  
48 chemical processes in the atmosphere (Gensch et al., 2014; Kawamura et al., 2004), as well as  
49 atmospheric composition in history (Dean et al., 2014). However, studies based on single isotope  
50 analysis have their limitations (Meier-Augenstein and Kemp, 2012). Those include an uncertainty when  
51 multiple sources or different processes are present, whose measured delta values may overlap (typically  
52 in the narrower  $\delta^{13}\text{C}$  range). Another factor are isotope fractionation processes which may compromise  
53 the accuracy of source identification (Xue et al., 2009). Using isotope analysis on multiple phases (gas  
54 and particulate matter) or multiple isotope analysis can overcome these problems and may be useful to  
55 constrain the potential sources/processes.

56 Generally, isotopic composition is affected by both primary emissions (e.g., Heaton, 1990; Widory,  
57 2006) and secondary processes (e.g., Fisseha et al., 2009b; Walters et al., 2015a). Isotopes are  
58 furthermore altered mainly by kinetic and/or equilibrium fractionation processes. Kinetic isotope effects  
59 (KIE) occur mainly during unidirectional (irreversible) reactions but also diffusion or during reversible  
60 reactions that are not yet at equilibrium (Gensch et al., 2014). Owing to KIE, reaction products (both  
61 gasses and particles) are depleted in the heavy isotope relatively to the reactants, and this effect is  
62 generally observed in organic compounds (Irei et al., 2006). If the partitioning between phases is caused  
63 by non-equilibrium processes (such as e.g. absorption), the isotopic fractionation is small and lower  
64 than that caused by chemical reactions (Rahn and Eiler, 2001). Equilibrium isotope effects occur in  
65 reversible chemical reactions or phase changes if the system is in equilibrium. Under such conditions,  
66 the heavier isotope is bound into the compounds where the total energy of the system is minimized and  
67 the most stable. Equilibrium effects are typical for inorganic species and usually temperature dependent.  
68 Regarding to the isotopic distribution in individual phases,  $^{15}\text{N}$  is generally depleted in gas phase  
69 precursors (ammonia, nitrogen oxides) but is more enriched in ions ( $\text{NH}_4^+$ ,  $\text{NO}_3^-$ ) in rainfall and the  
70 most enriched in particulate matter and dry deposition (Heaton et al., 1997; Ti et al., 2018). Total

71 nitrogen usually consists of the three main components,  $\text{NO}_3^-$ ,  $\text{NH}_4^+$  and/or organic nitrogen (OrgN),  
72 and thus, the final  $\delta^{15}\text{N}$  value in TN can be formulated by the following equation:

$$73 \delta^{15}\text{N}_{\text{TN}} = \delta^{15}\text{N}_{\text{NO}_3^-} * f_{\text{NO}_3^-} + \delta^{15}\text{N}_{\text{NH}_4^+} * f_{\text{NH}_4^+} + \delta^{15}\text{N}_{\text{OrgN}} * f_{\text{OrgN}}$$

74 where  $f_{\text{NO}_3^-} + f_{\text{NH}_4^+} + f_{\text{OrgN}} = 1$  and  $f$  represents the fractions of nitrogen from  $\text{NO}_3^-$ ,  $\text{NH}_4^+$  and OrgN in  
75 TN, respectively.

76 Total carbon in aerosol is usually divided into elemental carbon (EC) and organic carbon (OC), where  
77 OC forms the major part of TC (e.g., Mbengue et al., 2018). Although EC is more or less inert to  
78 chemical changes, slightly different  $\delta^{13}\text{C}$  in EC originating from primary emissions are described  
79 (Kawashima and Haneishi, 2012). OC represents a wide variety of organic compounds which can  
80 originate from different sources with different  $^{13}\text{C}$  content resulting in different  $\delta^{13}\text{C}$  values in bulk of  
81 emissions. Changes in isotopic ratio of  $\delta^{13}\text{C}$  in OC (and thus also TC) can subsequently affect chemical  
82 reactions where isotope fractionations via the kinetic isotope effect (KIE) usually dominate the  
83 partitioning between gas and aerosol (liquid/solid) phases (e.g. Zhang et al., 2016).

84  
85 Many studies have been conducted on  $\delta^{13}\text{C}$  and  $\delta^{15}\text{N}$  in particulate matter (PM) in Asia (e.g., Kundu et  
86 al., 2010; Pavuluri et al., 2015b; Pavuluri and Kawamura, 2017) and the Americas (e.g., Martinelli et  
87 al., 2002; Savard et al., 2017). Recently, the multiple isotope approach was applied in several studies  
88 by using  $\delta^{13}\text{C}$  and  $\delta^{15}\text{N}$  measurements. Specifically, the  $\delta^{13}\text{C}$  and  $\delta^{15}\text{N}$  composition of aerosol (along  
89 with other supporting data) was used to identify the sources and processes on marine sites in Asia  
90 (Bikkina et al., 2016; Kunwar et al., 2016; Miyazaki et al., 2011; Xiao et al., 2018). Same isotopes were  
91 used to determine the contribution of biomass burning to organic aerosols in India (Boreddy et al., 2018)  
92 and in Tanzania (Mkoma et al., 2014), or to unravel the sources of aerosol contamination at Cuban rural  
93 and urban coastal sites (Morera-Gómez et al., 2018). These studies show the potential advantages of  
94  $\delta^{13}\text{C}$  and  $\delta^{15}\text{N}$  isotope ratios to characterize aerosol types and to reveal the underlying chemical  
95 processes that take place in them.

96 Only few studies on  $\delta^{13}\text{C}$  and  $\delta^{15}\text{N}$  isotope ratios have been performed in Europe, which are moreover  
97 often based on single isotope analysis. Regarding the isotopes of nitrogen, Widory (2007) published a  
98 broad study on  $\delta^{15}\text{N}$  in TN in PM10 samples from Paris, focusing on seasonality (winter vs. summer)  
99 with some specific sources. Freyer (1991) reported the seasonal variation in the  $\delta^{15}\text{N}$  of nitrate in  
100 aerosols and rainwater as well as gaseous  $\text{HNO}_3$  at a moderately polluted urban area in Jülich (Germany).  
101 Yeatman et al. (2001a, 2001b) conducted analyses of  $\delta^{15}\text{N}$  in  $\text{NO}_3^-$  and  $\text{NH}_4^+$  at two coastal sites from  
102 Weybourne, England, and Mace Head, Ireland, focusing on the effects of the possible sources and  
103 aerosol size segregation on their formation processes and isotopic enrichment. More recently, Ciężka  
104 et al. (2016) reported one-year observations of  $\delta^{15}\text{N}$  in  $\text{NH}_4^+$  and ions in precipitation at an urban site  
105 in Wrocław, Poland, whereas Beyn et al. (2015) reported seasonal changes in  $\delta^{15}\text{N}$  in  $\text{NO}_3^-$  in wet and  
106 dry deposition at a coastal and an urban site in Germany to evaluate the nitrogen pollution levels.

107 Studies on  $\delta^{13}\text{C}$  at European sites have been focused more on urban aerosols. Fisseha et al. (2009) used  
108 stable carbon isotopes of the different carbonaceous aerosol fractions (TC, black carbon, and water  
109 soluble and insoluble OC) to determine the sources of urban aerosols in Zurich, Switzerland, during  
110 winter and summer. Similarly, Widory et al. (2004) used  $\delta^{13}\text{C}$  of TC, along with an analysis of lead  
111 isotopes, to study the origin of aerosol particles in Paris (France). Górká et al. (2014) used  $\delta^{13}\text{C}$  in TC  
112 in conjunction with PAH analyses for the determination of the sources of PM10 organic matter in  
113 Wrocław, Poland, during vegetative and heating seasons. Masalaite et al. (2015) used an analysis of  
114  $\delta^{13}\text{C}$  in TC on size-segregated urban aerosols to elucidate carbonaceous PM sources in Vilnius,  
115 Lithuania. Fewer studies have been conducted on  $\delta^{13}\text{C}$  in aerosols in rural and remote areas of Europe.  
116 In the 1990s, Pichlmayer et al. (1998) conducted a multiple isotope analysis of  $\delta^{13}\text{C}$  in OC,  $\delta^{15}\text{N}$  in  $\text{NO}_3^-$   
117 and  $\delta^{34}\text{S}$  in  $\text{SO}_4^{2-}$  in snow and air samples for the characterization of pollutants at high-alpine sites in  
118 Central Europe. Recently, Martinsson et al. (2017) published seasonal observations of  $\delta^{13}\text{C}$  in TC, along  
119 with the  $^{14}\text{C}/^{12}\text{C}$  isotope ratio of PM10 at a rural background station in Vavahill in southern Sweden  
120 based on 25 weekly samples.

121 To broaden the multiple isotope approach over the European continent, we present seasonal variations  
122 in  $\delta^{13}\text{C}$  of TC and  $\delta^{15}\text{N}$  of TN in the PM1 fraction of atmospheric aerosols at a rural background site in  
123 Central Europe. To the best of our knowledge, this is the first seasonal study of these isotopes in this  
124 region, and it is one of the most comprehensive isotope studies of fine aerosol fraction.

125

## 126 **2. Materials and methods**

### 127 **2.1. Measurement site**

128

129 The Košetice observatory is a key station of the Czech Hydrometeorological Institute (CHMI), focusing  
130 on air quality and environmental monitoring (Váňa and Dvorská, 2014). The site is located in the Czech  
131 Highlands (49°34'24.13" N, 15°4'49.67" E, 534 m ASL) and is surrounded by an agricultural landscape  
132 and forests, out of range of major sources of pollution with very low traffic density. The observatory is  
133 officially classified as a Central European rural background site, which is part of the EMEP, ACTRIS,  
134 and GAW networks. A characterization of the station in terms of the chemical composition of fine  
135 aerosols during different seasons and air masses is presented by Schwarz et al. (2016) and longtime  
136 trends by Mbengue et al. (2018) and Pokorná et al. (2018). As part of a monitoring network operated  
137 by the CHMI, the site is equipped with an automated monitoring system that provides meteorological  
138 data (wind speed and direction, relative humidity, temperature, pressure, and solar radiation) and the  
139 concentrations of gaseous pollutants ( $\text{SO}_2$ , CO, NO,  $\text{NO}_2$ ,  $\text{NO}_x$  and  $\text{O}_3$ ).

140

## 2.2. Sampling and weighing

Aerosol samples were collected every two days for 24 h from September 27, 2013, to August 9, 2014, using a Leckel sequential sampler SEQ47/50 equipped with a PM1 sampling inlet. Some temporal gaps were caused by sampler maintenance or power outages resulting in 146 samples during the almost year-long study. The sampler was loaded with pre-baked (3 h, 800°C) quartz fiber filters (Tissuequartz, Pall, 47 mm), and operated at a flow rate of 2.3 m<sup>3</sup>/h. In addition, field blanks (n = 7) were also taken for an analysis of the contribution of adsorbed organic vapors (positive artefact).

The PM1 was measured gravimetrically (each filter before and after the sampling) with a microbalance that had ±1 µg sensitivity (Sartorius M5P, Sartorius AG, Göttingen, Germany) in a controlled environment (20±1 °C and 50±3 % relative humidity after filter equilibration for 24 h).

## 2.3. Determination of TC, TN concentrations and their stable isotopes

For the measurements of total carbon (TC) and nitrogen (TN) and their stable isotope ratios, small filter discs (area 0.5 cm<sup>2</sup>, 1.13 cm<sup>2</sup> or 2.01 cm<sup>2</sup>) were placed in a pre-cleaned tin cup, shaped into a small marble using a pair of tweezers, and introduced into the elemental analyzer (EA; Flash 2000, Thermo Fisher Scientific) using an autosampler. Inside the EA, samples were first oxidized in a quartz column heated at 1000°C, in which the tin marble burns and oxidizes all the carbon and nitrogen species to CO<sub>2</sub> and nitrogen oxides, respectively. In the second quartz column, heated to 750°C, nitrogen oxides were reduced to N<sub>2</sub>. Evolved CO<sub>2</sub> and N<sub>2</sub> were subsequently separated on a gas chromatographic column, which was installed in EA, and measured with a thermal conductivity detector for TC and TN. CO<sub>2</sub> and N<sub>2</sub> were then transferred into an isotope ratio mass spectrometer (IRMS; Delta V, Thermo Fisher Scientific) through a ConFlo IV interface to monitor the <sup>15</sup>N/<sup>14</sup>N and <sup>13</sup>C/<sup>12</sup>C ratios.

An acetanilide external standard (from Thermo Electron Corp.) was used to determine the calibration curves before every set of measurements for calculating TC, TN and their isotope values. The δ<sup>15</sup>N and δ<sup>13</sup>C values of the acetanilide standard were 11.89‰ (relative to the atmospheric nitrogen) and -27.26‰ (relative to Vienna Pee Dee Belemnite standard), respectively. Subsequently, the δ<sup>15</sup>N of TN and δ<sup>13</sup>C of TC were calculated using the following equations and the final δ values are expressed in relation to the international standards:

$$\delta^{15}\text{N} (\text{‰}) = \left[ \frac{(^{15}\text{N}/^{14}\text{N})_{\text{sample}}}{(^{15}\text{N}/^{14}\text{N})_{\text{standard}}} - 1 \right] * 1000$$

$$\delta^{13}\text{C} (\text{‰}) = \left[ \frac{(^{13}\text{C}/^{12}\text{C})_{\text{sample}}}{(^{13}\text{C}/^{12}\text{C})_{\text{standard}}} - 1 \right] * 1000$$

## 177        **2.4.    Ion chromatography**

178

179    The loads on the quartz filters was further analyzed by using a Dionex ICS-5000 (Thermo Scientific,  
180    USA) ion chromatograph (IC). The samples were extracted using ultrapure water with conductivity  
181    below 0.08  $\mu\text{S}/\text{m}$  (Ultrapur, Watrex Ltd., Czech Rep.) for 0.5 h using an ultrasonic bath and 1 h using  
182    a shaker. The solution was filtered through a Millipore syringe filter with 0.22  $\mu\text{m}$  porosity. The filtered  
183    extracts were then analyzed for both anions ( $\text{SO}_4^{2-}$ ,  $\text{NO}_3^-$ ,  $\text{Cl}^-$ ,  $\text{NO}_2^-$  and oxalate) and cations ( $\text{Na}^+$ ,  $\text{NH}_4^+$ ,  
184     $\text{K}^+$ ,  $\text{Ca}^{2+}$  and  $\text{Mg}^{2+}$ ) in parallel. The anions were analyzed using an anion self-regenerating suppressor  
185    (ASRS 300) and an IonPac AS11-HC (2 x 250 mm) analytical column and measured with a Dionex  
186    conductivity detector. For cations, a cation self-regenerating suppressor (CSRS ULTRA II) and an  
187    IonPac CS18 (2 m x 250 mm) analytical column were used in conjunction with a Dionex conductivity  
188    detector. The separation of anions was conducted using 25 mM KOH as an eluent at a flow rate of 0.38  
189    ml/min, and the separation of cations was conducted using 25 mM methanesulfonic acid at 0.25 ml/min.

190

191    The sum of nitrate and ammonium nitrogen showed a good agreement with the measured TN (Fig. S1  
192    in Supplementary Information (SI)), and based on the results of TN,  $\text{NO}_3^-$  and  $\text{NH}_4^+$ , organic nitrogen  
193    (OrgN) was also calculated using the following equation (Wang et al., 2010):  $\text{OrgN} = \text{TN} - 14 \cdot [\text{NO}_3^-$   
194     $/62 + \text{NH}_4^+/18]$ .

195

## 196        **2.5.    EC/OC analysis**

197

198    Online measurements of organic and elemental carbon (OC and EC) were obtained from parallel  
199    sampling on quartz filters by a field semi-online OC/EC analyzer (Sunset Laboratory Inc., USA)  
200    connected to a PM1 inlet. The instrument was equipped with a carbon parallel-plate denuder (Sunset  
201    Lab.) to remove volatile organic compounds to avoid a positive bias in the measured OC. Samples were  
202    taken at 4 h intervals, including the thermal-optical analysis, which lasts approximately 15 min. The  
203    analysis was performed using the shortened EUSAAR2 protocol: step [gas] temperature [ $^{\circ}\text{C}$ ]/duration  
204    [s]: He 200/90, He 300/90, He 450/90, He 650/135, He-Ox. 500/60, He-Ox. 550/60, He-Ox. 700/60,  
205    He-Ox. 850/100 (Cavalli et al., 2010). Automatic optical corrections for charring were made during  
206    each measurement, and a split point between EC and OC was detected automatically (software:  
207    RTCalc526, Sunset Lab.). Instrument blanks were measured once per day at midnight, and they  
208    represent only a background instrument response without filter exposure. Control calibrations using a  
209    sucrose solution were made before each change of the filter (ca. every 2<sup>nd</sup> week) to check the stability  
210    of instruments. The 24 h averages with identical measuring times, such as on quartz filters, were  
211    calculated from the acquired 4 h data. The sum of EC and OC provided TC concentrations, which were  
212    consistent with the TC values measured by EA (see Fig. S2 in SI).

213

## 214 **2.6. Spearman correlation calculations**

215

216 Spearman correlation coefficients ( $r$ ) were calculated using R statistical software (ver. 3.3.1). The  
217 correlations were calculated for the annual dataset ( $n=139$ , without the winter *Event* samples) and  
218 separately for each season (autumn: 25, winter: 38, spring: 43, and summer: 33), and winter event (7).  
219 Data from the winter *Event* were excluded from the annual and winter datasets for the correlation  
220 analysis as their distinctly high concentrations and isotopic values might have affected the results.  
221 Correlations with  $p$ -values  $< 0.05$  were taken as statistically insignificant.

222

## 223 **3. Results and discussion**

224

225 The time series of TN, TC and their isotope ratios ( $\delta^{15}\text{N}$  and  $\delta^{13}\text{C}$ ) for the whole measurement campaign  
226 are depicted in Fig. 1. Some sampling gaps were caused in autumn and at the end of spring by servicing  
227 or outages of the sampler. However, 146 of the samples from September 27, 2013, to August 9, 2014  
228 are sufficient for a seasonal study. In Fig. 1, the winter *Event* is highlighted, which has divergent values,  
229 especially for  $\delta^{15}\text{N}$ , and is discussed in detail in section 3.4.

230

231 Table 1 summarizes the results for four seasons: autumn (Sep.–Nov.), winter (Dec.–Feb.), spring (Mar.–  
232 May) and summer (Jun.–Aug.). The higher TN concentrations were observed in spring (max.  $7.59 \mu\text{gN}$   
233  $\text{m}^{-3}$ ), while the higher TC concentrations were obtained during the winter *Event* (max.  $13.6 \mu\text{gC m}^{-3}$ ).  
234 Conversely, the lowest TN and TC concentrations were observed in summer (Tab. 1).

235

236 Figure 2 shows the relationships between the TC and TN concentrations and their stable isotopes for  
237 one year. The correlation between TC and TN is significant ( $r=0.71$ ), but the relationship split during  
238 high concentration events due to divergent sources. The highest correlations between TC and TN were  
239 obtained during transition periods in autumn (0.85) and spring (0.80). Correlations between TC and TN  
240 in winter (0.43) and summer (0.37) were weaker but still statistically significant ( $p<0.05$ ). As seen in  
241 Table 1, the seasonal averages of TC/TN ratios fluctuate, but their medians have similar values for  
242 autumn, winter and spring. The summer TC/TN value is higher (3.45) and characteristic of a significant  
243 shift in chemical composition, which is in line with previous studies at the site (Schwarz et al., 2016).  
244 However, seasonal differences in the TC/TN ratios were not as large as those in other works (e.g.,  
245 Agnihotri et al., 2011), and thus, this ratio itself did not provide much information about aerosol sources.

246

247 The correlation between  $\delta^{13}\text{C}$  and  $\delta^{15}\text{N}$  (Fig. 2, right) is also significant but negative (-0.69). However,  
248 there is a statistically significant correlation for spring only (-0.54), while in other seasons, correlations  
249 are statistically insignificant. This result highlights a significant shift in the sources of carbonaceous  
250 aerosols and their isotope values in spring while the sources were rather stable during other seasons.  
251 The winter *Event* measurements show the highest  $\delta^{13}\text{C}$  and lowest  $\delta^{15}\text{N}$  values, but a linear fit does not  
252 show a significant differences as compared to rest of the data (Fig. 2, right).

253

### 254 3.1. Total nitrogen and its $\delta^{15}\text{N}$

255

256 The  $\delta^{15}\text{N}$  values are stable in winter at approximately 15‰, with an exception of winter *Event*, which  
257 showed an average of 13‰. In summer, the  $\delta^{15}\text{N}$  shows strong enrichment of  $^{15}\text{N}$  in comparison with  
258 winter, resulting in an average value of 25‰. During the spring period, we observed a slow increase in  
259  $\delta^{15}\text{N}$  from April to June (Fig. 1), indicating a gradual change in nitrogen chemistry in the atmosphere.  
260 During autumn, a gradual change is not obvious because of a lack of data in a continuous time series.  
261 The range of  $\delta^{15}\text{N}$  was from 0.6‰ to 28.2‰ year round. Such a wide range may arise from a limited  
262 number of nitrogen-containing species and/or components in aerosols, which are specifically present in  
263 the forms of  $\text{NO}_3^-$ ,  $\text{NH}_4^+$  and/or organic nitrogen (OrgN). The highest portion of nitrogen is contained  
264 in  $\text{NH}_4^+$  (54 % of TN year-round), followed by OrgN (27 %) and  $\text{NO}_3^-$  (19 %). Although the  $\text{NH}_4^+$   
265 content in TN is seasonally stable (51-58 %, Table 1), the  $\text{NO}_3^-$  content is seasonally dependent; the  
266 highest in winter, and somewhat lower in spring and autumn. In summer when the dissociation of  
267  $\text{NH}_4\text{NO}_3$  plays an important role the  $\text{NO}_3^-$  content is very low and its nitrogen is partitioned from the  
268 aerosol phase to gas phase (Stelson et al., 1979).

269

270 The seasonal trend of  $\delta^{15}\text{N}$  of TN, with the lowest values in winter and highest in summer, has been  
271 observed in other studies from urban Paris (Widory, 2007), rural Brazil (Martinelli et al., 2002), East  
272 Asian Jeju Island (Kundu et al., 2010) and rural Baengnyeong Island (Park et al., 2018) sites in Korea.  
273 However, different seasonal trends of  $\delta^{15}\text{N}$  of TN in Seoul (Park et al., 2018) show that such seasonal  
274 variation does not always occur.

275

276 Figure 3 shows changes in  $\delta^{15}\text{N}$  values as a function of the main nitrogen components in TN, with  
277 different colors for different days. There are two visible trends for a type of nitrogen. Although  $^{15}\text{N}$  is  
278 more depleted with increasing contents of  $\text{NO}_3^-$  in TN, the opposite is true for  $\text{NH}_4^+$  and OrgN. The  
279 strongest dependence for most bulk data is expressed by a strong negative correlation between  $\delta^{15}\text{N}$  and  
280 the fraction of  $\text{NO}_3^-$  in TN (Fig. 3). In all cases, the dependence during the winter *Event* is completely  
281 opposite to the rest of the bulk data (Fig. 3), suggesting the presence of different processes for  $\delta^{15}\text{N}$

282 values, which is characterized by a strong positive correlation between  $\delta^{15}\text{N}$  and  $\text{NO}_3^- \text{-N/TN}$  (0.98).  
283 This point will be discussed in section 3.4.

284

285 Considering the individual nitrogen components, several studies (Freyer, 1991; Kundu et al., 2010;  
286 Yeatman et al., 2001b) showed seasonal trends of  $\delta^{15}\text{N}$  of  $\text{NO}_3^-$ , with the lowest  $\delta^{15}\text{N}$  in summer and the  
287 highest in winter. Savard et al. (2017 and references therein) summarized four possible reasons for this  
288 seasonality of  $\delta^{15}\text{N}$  of  $\text{NO}_3^-$ ; namely, (i) changes in  $\text{NO}_x$  emissions, (ii) influence of wind directions in  
289 the relative contributions from sources with different isotopic compositions, (iii) the effect of  
290 temperature on isotopic fractionation and (iv) chemical transformations of nitrogen oxides over time  
291 with a lower intensity of sunlight, which can lead to higher  $\delta^{15}\text{N}$  values of atmospheric nitrate during  
292 winter months, as shown by Walters et al. (2015a). In our study, it is most likely that all these factors  
293 contributed, to a certain extent, to the nitrogen isotopic composition of  $\text{NO}_3^-$  throughout the year.

294

295 Conversely, Kundu et al. (2010) reported higher  $\delta^{15}\text{N}$  values of  $\text{NH}_4^+$  in summer than in winter and  
296 reported higher  $\delta^{15}\text{N}$  values of  $\text{NH}_4^+$  than  $\text{NO}_3^-$ , except for winter season. In sum, the contribution of  
297  $\text{NH}_4^+$  to  $\delta^{15}\text{N}$  overwhelms that of  $\text{NO}_3^-$ . Additionally, TN is composed of  $\text{NH}_4^+$ ,  $\text{NO}_3^-$  and OrgN. In  
298 Figure 3, we can observe an enrichment of  $^{15}\text{N}$  in TN in summer when the lowest  $\text{NO}_3^-$  contribution  
299 occurs. Thus, higher  $\delta^{15}\text{N}$  values of TN in summer are mainly caused by higher abundances of  $\text{NH}_4^+$   
300 originating from  $(\text{NH}_4)_2\text{SO}_4$ , OrgN and ammonium salts of organic acids.

301

302 Furthermore, we observed one of the largest enrichments of  $^{15}\text{N}$  of TN in summer aerosols as compared  
303 to previous studies (Kundu et al., 2010 and references therein), which may be explained by several  
304 reasons. First, the previous studies mainly focused on total suspended particles (TSP); however, we  
305 focused on the fine fraction (PM1), whose surface should be more reactive due to a larger surface area  
306 per unit of aerosol mass than the coarse fraction and consequently result in a higher abundance of  $^{15}\text{N}$   
307 during the gas/particle partitioning between  $\text{NH}_3$  and  $\text{NH}_4^+$ . Second, fine accumulation mode particles  
308 have a longer residence time in the atmosphere than the coarse mode fraction, which is also a factor  
309 that results in an enrichment of  $^{15}\text{N}$ . Indeed, Mkoma et al. (2014) reported average higher  $\delta^{15}\text{N}$  of TN  
310 in fine (17.4‰, PM2.5) than coarse aerosols (12.1‰, PM10). Freyer (1991) also reported higher  $\delta^{15}\text{N}$   
311 of  $\text{NO}_3^-$  (4.2‰ to 8‰) in fine aerosols (< 3.5  $\mu\text{m}$ ) in comparison with the coarse mode (-1.4‰ to 5.5‰).  
312 Third, a shorter sampling interval of our work (24 h) leads to higher chance of collecting episodic  
313 samples such as the winter *Event*, which could not be clearly detected due to averaged (overlapped)  
314 aerosols over a longer sampling period (e.g., weekly samples).

315

316 Similarly, as in this study, the highest  $\delta^{15}\text{N}$  values in TN were observed in a few studies from the Indian  
317 region (Aggarwal et al., 2013; Bikkina et al., 2016; Pavuluri et al., 2010) where biomass burning is the  
318 common source, and ambient temperatures are high. Therefore, in addition to the above reasons,

319 temperature also plays a significant role in  $^{15}\text{N}$  enrichment. This point will be discussed in more detail  
320 in section 3.3.

321

322 Figure 4 shows the  $\delta^{15}\text{N}$  of TN as a function of  $\text{NO}_3^-$  concentration. Samples with the highest  $\text{NO}_3^-$   
323 concentrations ( $>6 \mu\text{g m}^{-3}$ ,  $n=5$ ) show an average  $\delta^{15}\text{N}$  of  $13.3 \pm 0.7\text{‰}$ . Assuming that  $\text{NO}_3^-$  in the fine  
324 aerosol fraction consists predominantly of  $\text{NH}_4\text{NO}_3$  (Harrison and Pio, 1983), it can be stated that  
325 ammonium nitrate is a source of nitrogen at the Košetice site, with  $\delta^{15}\text{N}$  values at approximately 13.3‰,  
326 which is similar to the winter values of  $\delta^{15}\text{N}$  in  $\text{NO}_3^-$  in other studies. Specifically, Kundu et al. (2010)  
327 reported a winter average of  $\delta^{15}\text{N}$  of  $\text{NO}_3^-$  at  $+15.9\text{‰}$  from a Pacific marine site at Gosan Island, South  
328 Korea, whereas Freyer (1991) reported  $+9.2\text{‰}$  in a moderately polluted site from Jülich, Germany.  
329 Yeatman et al. (2001) reported approximately  $+9\text{‰}$  from a Weybourne coastal site, UK. Park et al.  
330 (2018) reported 11.9‰ in Seoul and 11.7‰ from a rural site in Baengnyeong Island, Korea.

331

332 Considering the  $\delta^{15}\text{N}$  of nitrogen oxides, which are common precursors of particulate nitrate, we can  
333 see that the  $\delta^{15}\text{N}$  of nitrogen oxides generated by coal combustion (Felix et al., 2012;  $+6$  to  $+13\text{‰}$ ,  
334 Heaton, 1990) or biomass burning ( $+14\text{‰}$ , Felix et al., 2012) are in the same range with our  $\delta^{15}\text{N}$  during  
335 the period of enhanced concentrations of  $\text{NO}_3^-$ . These  $\delta^{15}\text{N}$  values of nitrogen oxides are also  
336 significantly higher than those from vehicular exhaust ( $-13$  to  $-2\text{‰}$  Heaton, 1990;  $-19$  to  $+9\text{‰}$  Walters  
337 et al., 2015b) or biogenic soil ( $-48$  to  $-19\text{‰}$ , Li and Wang, 2008). Because of the only slight difference  
338 between above reported  $\delta^{15}\text{N}$  of nitrogen oxides and our  $\delta^{15}\text{N}$  of TN during maximal  $\text{NO}_3^-$  events, the  
339 isotope composition is probably influenced by the process of kinetic isotopic fractionation in fossil fuel  
340 combustion samples during heating season as referred by Cieżka et al. (2016) as one of three possible  
341 processes. Thus,  $\delta^{15}\text{N}$  values around 13.3‰ (Fig. 4) are probably characteristic of fresh emissions from  
342 heating (both coal and biomass burning) because these values are obtained during the domestic heating  
343 season.

344

345 The exponential curves in Fig. 4 represent a boundary in which  $\delta^{15}\text{N}$  values are migrating as a result of  
346 the enrichment or depletion of  $^{15}\text{N}$ , which is associated with the removal or loading of  $\text{NO}_3^-$  in aerosols.  
347 These curves represent two opposite chemical processes converting on approximately 13.3‰, which  
348 showed a strong logarithmic correlation ( $r=0.96$  during winter *Event*, green line, and  $-0.81$  for the rest  
349 of points, black line, Fig. S3). These results indicate a significant and different mechanism by which  
350 nitrogen isotopic fractionation occurs in aerosols. In both cases, the decrease in nitrate leads to  
351 exponential changes in the enrichment or depletion of  $^{15}\text{N}$  from a value of 13.3‰. In the case of  
352 enrichment, in addition to a higher proportion of  $\text{NH}_4^+$  than  $\text{NO}_3^-$ , the dissociation process of  $\text{NH}_4\text{NO}_3$   
353 can cause an increase in  $^{15}\text{N}$  of TN during a period of higher ambient temperatures, as hypothesized by  
354 Pavuluri et al. (2010).

355

356 OrgN has not been widely studied as compared to particulate  $\text{NO}_3^-$  and  $\text{NH}_4^+$ , although it represents a  
357 significant fraction of TN (e.g., Jickells et al., 2013; Neff et al., 2002; Pavuluri et al., 2015). Figure 5  
358 shows the relationship between  $\delta^{15}\text{N}$  of TN and OrgN. Organic nitrogen consists organic compounds  
359 containing nitrogen in water soluble and insoluble fractions. The majority of samples have a  
360 concentration range of 0.1-0.5  $\mu\text{g m}^{-3}$  (gray highlight in Fig. 5), which can be considered as background  
361 OrgN at the Košetice site. During the domestic heating season with the highest concentrations of  $\text{NO}_3^-$   
362 and  $\text{NH}_4^+$ , we can observe a significant increase in OrgN with  $\delta^{15}\text{N}$  again at approximately 13.3‰,  
363 which implies that the isotopic composition of OrgN is determined by the same source. In the case of  
364 emissions from combustion, OrgN originates mainly from biomass burning (Jickells et al., 2013 and  
365 references therein), and thus, elevated concentrations of OrgN (as well as high  $\text{NO}_3^-$  and  $\text{NH}_4^+$  conc.)  
366 may refer to this source. On the other hand, looking at the trend of OrgN/TN vs.  $\delta^{15}\text{N}$  (Fig. 3), it is more  
367 similar to the trend of  $\text{NH}_4^+$ -N/TN than  $\text{NO}_3^-$ -N/TN. Thus, it can be considered that the changes in the  
368  $\delta^{15}\text{N}$  of OrgN in samples highlighted as a gray area in Fig. 5 are probably driven more by the same  
369 changes in  $\text{NH}_4^+$  particles, and especially in summer with elevated OrgN in TN (Table 1).  
370

### 371 **3.2. Total carbon and its $\delta^{13}\text{C}$**

372  
373 The  $\delta^{13}\text{C}$  of TC ranged from -28.9 to -25.4‰ (Fig. 6) and the lowest  $\delta^{13}\text{C}$  we observed in field blank  
374 samples (mean -29.2‰, n=7), indicating that the lowest summer values in particulate matter were close  
375 to gas phase values. Our  $\delta^{13}\text{C}$  values are within the range reported for particulate TC (-29‰ to -15‰)  
376 as summarized by Gensch et al. (2014). The lowest values are associated with fine particles after  
377 combustion and transport (Ancelet et al., 2011; Widory, 2006) while the highest values are associated  
378 with the coarse fraction and carbonate contribution (Kawamura et al., 2004). This broad range can be  
379 explained by the influence of marine aerosols (Ceburnis et al., 2016), different anthropogenic sources  
380 (e.g., Widory et al., 2004), as well as different distributions of C3 and C4 plants (Martinelli et al., 2002)  
381 resulting in different  $\delta^{13}\text{C}$  values in the northern and southern hemispheres (Cachier, 1989). The  $\delta^{13}\text{C}$   
382 values at the Košetice site fall within the range common to other European sites. For example, a rural  
383 background site in Vavihill (southern Sweden, range -26.7 to -25.6‰, Martinsson et al. (2017)), urban  
384 Wroclaw (Poland, range -27.6 to -25.3‰, Górka et al. (2014)), different sites (urban, coastal, forest) in  
385 Lithuania (East Europe, Masalaite et al., 2015, 2017), as well as urban Zurich (Switzerland, Fisseha et  
386 al. (2009)).

387 The range of TC  $\delta^{13}\text{C}$  values is significantly narrower than that of TN  $\delta^{15}\text{N}$  due to a higher number of  
388 carbonaceous components in the aerosol mixture whose isotope ratio overlaps one another. However,  
389 it is possible to distinguish lower  $\delta^{13}\text{C}$  values in summer (Table 1), which may indicate a contribution  
390 from higher terrestrial plant emissions. Similarly, Martinsson et al. (2017) reported lower  $\delta^{13}\text{C}$  values

391 in summer in comparison with other seasons, which they explain by high biogenic aerosol contributions  
392 from C3 plants.

393 A similar dependence of  $\delta^{13}\text{C}$  on the TC concentration was observed by Fisseha et al. (2009), where  
394 winter  $^{13}\text{C}$  enrichment was associated with WSOC (water soluble organic carbon) that originated mainly  
395 from wood combustion. Similarly, at the Košetice station, different carbonaceous aerosols were  
396 observed during the heating season (Oct.–Apr.) than in summer (Mbengue et al., 2018; Vodička et al.,  
397 2015). Moreover, winter aerosols at the Košetice site were probably affected by not only biomass  
398 burning but also coal burning (Schwarz et al., 2016), which can result in higher carbon contents and  
399 more  $^{13}\text{C}$ -enriched particles (Widory, 2006). Furthermore, based on the number of size distribution  
400 measurements at the Košetice site, larger particles were observed in winter in comparison with summer,  
401 even in the fine particle fraction (Ziková and Ždímal, 2013), which can also have an effect on lower  
402  $\delta^{13}\text{C}$  values in summer. Thus, the relatively low  $\delta^{13}\text{C}$  values in our range (up to  $-28.9\text{‰}$ ) are because  
403 fine particles have lower  $\delta^{13}\text{C}$  values in comparison with coarse particles probably due to different  
404 sources of TC. (e.g., Masalaite et al., 2015; Skipitytė et al., 2016).

405

### 406 **3.3. Temperature dependence and correlations of $\delta^{15}\text{N}$ and $\delta^{13}\text{C}$ with other variables**

407

408 Tables 2 and 3 show Spearman's correlation coefficients ( $r$ ) of  $\delta^{15}\text{N}$  and  $\delta^{13}\text{C}$  with different variables  
409 that may reflect some effects on isotope distributions. In addition to year-round correlations,  
410 correlations for each season, as well as for the *Event*, are presented separately.

411

412 Correlations of  $\delta^{15}\text{N}$  in winter and summer are often opposite (e.g., for TN  $-0.40$  in winter vs.  $0.36$  in  
413 summer, for  $\text{NH}_4^+$   $-0.42$  in winter vs.  $0.40$  in summer), indicating that aerosol chemistry at the nitrogen  
414 level is different in these seasons. Similarly, the contradictory dependence between  $\delta^{15}\text{N}$  and TN in  
415 summer and winter was observed by Widory (2007) in PM10 samples from Paris. Widory (2007)  
416 connected this result with different primary nitrogen origin (road-traffic emissions in summer and no  
417 specific source in winter) and following secondary processes associated with isotope fractionation  
418 during degradation of atmospheric NO<sub>x</sub> leading to two distinct pathways for  $^{15}\text{N}$  enrichment (summer)  
419 and depletion (winter).

420

421 From a meteorological point of view, a significant correlation of  $\delta^{15}\text{N}$  with temperature has been  
422 obtained, indicating the influence of temperature on the nitrogen isotopic composition. The dependence  
423 of  $\delta^{15}\text{N}$  of TN on temperature (Fig. 7) is similar to that observed by Ciężka et al. (2016) for  $\delta^{15}\text{N}$  of  
424  $\text{NH}_4^+$  from precipitation; however, it is the opposite of that observed by Freyer (1991) for  $\delta^{15}\text{N}$  of  $\text{NO}_3^-$ .  
425 The aforementioned studies concluded that the isotope equilibrium exchange between nitrogen oxides  
426 and particulate nitrates is temperature dependent and could lead to more  $^{15}\text{N}$  enriched  $\text{NO}_3^-$  during the

427 cold season (Freyer et al., 1993; Savard et al., 2017). Although Savard et al. (2017) reported a similar  
428 negative temperature dependence for  $\delta^{15}\text{N}$  of  $\text{NH}_4^+$  in Alberta (Canada), most studies reported a positive  
429 temperature dependence for  $\delta^{15}\text{N}$  of  $\text{NH}_4^+$  that is stronger than that for  $\delta^{15}\text{N}$  of  $\text{NO}_3^-$  (e.g., Kawashima  
430 and Kurahashi, 2011; Kundu et al., 2010). The reason is that  $\text{NH}_3$  gas concentrations are higher during  
431 warmer conditions, and thus the isotopic equilibrium exchange reaction, i.e.,  $\text{NH}_3(\text{g}) \leftrightarrow \text{NH}_4^+(\text{p})$ , which  
432 leads to  $^{15}\text{N}$  enrichment in particles, is more intensive.

433

434 All the considerations mentioned above indicate that a resulting relationship between  $\delta^{15}\text{N}$  of TN and  
435 temperature is driven by the prevailing nitrogen species, which is  $\text{NH}_4^+$  in our case. A similar  
436 dependence was reported by Pavuluri et al. (2010) between temperature and  $\delta^{15}\text{N}$  of TN in Chennai  
437 (India), where  $\text{NH}_4^+$  strongly prevailed. They found the best correlation between  $\delta^{15}\text{N}$  and temperature  
438 during the colder period (range 18.4-24.5°C, avg. 21.2°C); however, during warmer periods, this  
439 dependence was weakened. In our study, we observed the highest correlation of  $\delta^{15}\text{N}$  with temperature  
440 in autumn ( $r=0.58$ , temp. range -1.9 to 13.9°C, avg. 6.6°C), followed by spring ( $r=0.52$ , temp. range  
441 1.5-18.7°C, avg. 9.3°C), but there was even a negative but insignificant correlation in summer (temp.  
442 range: 11.8-25.5°C, avg. 17.7°C). This result indicates that ambient temperature plays an important role  
443 in the enrichment/depletion of  $^{15}\text{N}$ ; however, it is not determined by a specific temperature range but  
444 rather the conditions for repeating the process of “evaporation/condensation”, as shown by the  
445 comparison with the work of Pavuluri et al. (2010). It is likely that isotopic fractionation caused by the  
446 equilibrium reaction of  $\text{NH}_3(\text{g}) \leftrightarrow \text{NH}_4^+(\text{p})$  reaches a certain level of enrichment under higher  
447 temperature conditions in summer.

448

449 In summer,  $\delta^{15}\text{N}$  correlates positively with  $\text{NH}_4^+$  ( $r=0.40$ ) and  $\text{SO}_4^{2-}$  (0.51), indicating a link with  
450  $(\text{NH}_4)_2\text{SO}_4$  that is enriched by  $^{15}\text{N}$  due to aging. Figure 8 shows an enrichment of  $^{15}\text{N}$  as a function of  
451 the molar ratio of  $\text{NH}_4^+/\text{SO}_4^{2-}$ . The highest  $\text{NH}_4^+/\text{SO}_4^{2-}$  ratios, showing an ammonia rich atmosphere,  
452 were observed during winter, late autumn and early spring along with high abundance of  $\text{NO}_3^-$  that is  
453 related to favorable thermodynamic conditions during heating season and enough ammonia in the  
454 atmosphere. Gradual decreasing molar ratios of  $\text{NH}_4^+/\text{SO}_4^{2-}$  during spring indicate a gradual increase of  
455 ambient temperatures and therefore worsened thermodynamic conditions for  $\text{NO}_3^-$  formation in aerosol  
456 phase, which was accompanied by a visible decrease in the nitrate content in aerosols (Fig. 8). The  
457 increase of temperatures finally leads to the  $\text{NH}_4^+/\text{SO}_4^{2-}$  ratio reaching 2 at the turn of spring and summer.  
458 Finally, summer values of  $\text{NH}_4^+/\text{SO}_4^{2-}$  molar ratio below 2 indicate that  $\text{SO}_4^{2-}$  in aerosol particles at high  
459 summer temperatures may not be completely saturated with ammonium but it can be composed from  
460 mixture of  $(\text{NH}_4)_2\text{SO}_4$  and  $\text{NH}_4\text{HSO}_4$  (Weber et al., 2016). The equilibrium reaction between these two  
461 forms of ammonium sulfates related to temperature oscillation during a day and due to vertical mixing  
462 of the atmosphere is a probable factor which leads to increased values of  $\delta^{15}\text{N}$  in early summer.  
463 Ammonia measurements, that were carried out at the Košetice site until 2001, showed that  $\text{NH}_3$

464 concentrations in summer were slightly higher than in winter  
465 ([http://portal.chmi.cz/files/portal/docs/uoco/isko/tab\\_roc/2000\\_enh/CZE/kap\\_18/kap\\_18\\_026.html](http://portal.chmi.cz/files/portal/docs/uoco/isko/tab_roc/2000_enh/CZE/kap_18/kap_18_026.html)),  
466 which supports temperature as a main factor influencing  $\text{NH}_4^+/\text{SO}_4^{2-}$  ratio at Košetice. In this context,  
467 we noticed that 25 out of 33 summer samples have molar ratios of  $\text{NH}_4^+/\text{SO}_4^{2-}$  below 2, and the  
468 remaining samples are approximately 2, and the relative abundance of  $\text{NO}_3^-$  in PM1 in those samples is  
469 very low (ca. 1.7 %).

470  
471 Recently, Silvern et al. (2017) reported that organic aerosols can play a role in modifying or retarding  
472 the achievement of  $\text{H}_2\text{SO}_4\text{-NH}_3$  thermodynamic equilibrium at  $\text{NH}_4^+/\text{SO}_4^{2-}$  molar ratios of less than 2,  
473 even when sufficient amounts of ammonia are present in gas phase. Thus, an interaction between  
474 sulfates and ammonia may be hindered due to the preferential reaction with aged aerosols coated with  
475 organics (Liggio et al., 2011). In thermodynamic equilibrium, partitioning between gas ( $\text{NH}_3$ ) and  
476 aerosol ( $\text{NH}_4^+$ ) phases should result in even larger  $\delta^{15}\text{N}$  values of particles in summer, however,  
477 measurements show a different situation. Summer  $\delta^{15}\text{N}$  values are highest but further enrichment was  
478 stopped. Moreover, we observed a positive (and significant) correlation between temperature and  $\delta^{13}\text{C}$   
479 ( $r=0.39$ ) only in summer, whereas the correlation coefficient of  $\delta^{15}\text{N}$  vs. temperature is statistically  
480 insignificant, suggesting that while values of  $\delta^{15}\text{N}$  reached their maxima, the  $\delta^{13}\text{C}$  can still grow with  
481 even higher temperatures due to the influence of organics in summer season.

482  
483 As seen in Table 3, summertime positive correlations of  $\delta^{13}\text{C}$  with ozone ( $r=0.66$ ) and temperature  
484 ( $0.39$ ) indicate oxidation processes that can indirectly lead to an enrichment of  $^{13}\text{C}$  in organic aerosols  
485 that are enriched with oxalic acid (Pavuluri and Kawamura, 2016). This result is also supported by the  
486 fact that the content of oxalate in PM1, measured by IC, was twice as high in spring and summer than  
487 in winter and autumn. The influence of temperature on  $\delta^{13}\text{C}$  in winter is opposite to that in summer.  
488 The negative correlation ( $-0.35$ ) in winter probably indicates more fresh emissions from domestic  
489 heating (probably coal burning) with higher  $\delta^{13}\text{C}$  values during cold season.

490  
491 The whole year temperature dependence on  $\delta^{13}\text{C}$  is the opposite of that observed for  $\delta^{15}\text{N}$  (Fig. 7, left),  
492 suggesting more  $^{13}\text{C}$ -depleted products in summer. This result is probably connected with different  
493 carbonaceous aerosols during winter (anthropogenic emissions from coal, wood and biomass burning  
494 with the enrichment of  $^{13}\text{C}$ ) in comparison with the summer season (primary biogenic and secondary  
495 organic aerosols with lower  $\delta^{13}\text{C}$ ) (Vodička et al., 2015). The data of  $\delta^{13}\text{C}$  in Fig. 7 are also more  
496 scattered, which indicates that in the case of carbon, the isotopic composition depends more on sources  
497 than on temperature.

498  
499 Correlations of  $\delta^{13}\text{C}$  with OC are significant in all seasons; they are strongest in spring and weakest in  
500 summer (Table 3). Correlations of  $\delta^{13}\text{C}$  with EC, whose main sources are combustion processes from

501 domestic heating and transportation, are significant ( $r=0.61-0.88$ ) only during the heating season  
502 (autumn–spring, see Table 3), while in summer the correlation is statistically insignificant (0.28). Thus,  
503 the isotopic composition of aerosol carbon at the Košetice station is not significantly influenced by EC  
504 emitted from transportation; otherwise the year-round correlation between  $\delta^{13}\text{C}$  and EC would suggest  
505 that transportation is significant source of EC in summer. This result can be biased by the fact that EC  
506 constitutes on average 19% of TC during all seasons. However, it is consistent with positive correlations  
507 between  $\delta^{13}\text{C}$  and gaseous  $\text{NO}_2$ , as well as particulate nitrate, which is also significant in autumn to  
508 spring. This result is also supported by the negative correlation of  $\delta^{13}\text{C}$  with the EC/TC ratio ( $r=-0.51$ ),  
509 which is significant only in summer.

510

511 It should be mentioned that the wind directions during the campaign were similar, with the exception  
512 of winter season, when southeast (SE) winds prevailed (see Fig. S4 in SI). We did not observe any  
513 specific dependence of isotopic values on wind directions, except for the *Event*.

#### 514 **3.4. Winter Event**

515

516 The winter *Event* represents the period from January 23 to February 5, 2014, when an enrichment of  
517  $^{13}\text{C}$  and substantial depletion of  $^{15}\text{N}$  occurred in PM1 (see Figs. 1 and 9 for details). We do not observe  
518 any trends of the isotopic compositions of  $\delta^{15}\text{N}$  and  $\delta^{13}\text{C}$  with wind directions, except for the period of  
519 the *Event* and one single measurement on December 18, 2013. Both the *Event* and the single  
520 measurement are connected to SE winds through Vienna and the Balkan Peninsula (Fig. 10). More  
521 elevated wind speeds with very stable SE winds are observed on the site with samples showing the most  
522  $^{15}\text{N}$  depleted values at the end of the *Event* (Fig. 9). Stable weather conditions and the homogeneity of  
523 the results indicate a local or regional source, which is probably associated with the formation of sulfates  
524 (Fig. S5).

525

526 Although the *Event* contains only 7 samples, high correlations are obtained for  $\delta^{15}\text{N}$  and  $\delta^{13}\text{C}$  (Tables 2  
527 and 3). Generally, correlations of  $\delta^{15}\text{N}$  with several parameters during the *Event* are opposite to those  
528 of four seasons, indicating the exceptional nature of these aerosols from a chemical point of view.  
529 During the *Event*,  $\delta^{15}\text{N}$  correlates positively with  $\text{NO}_3^-$  ( $r=0.96$ ) and  $\text{NO}_3^- \text{-N/TN}$  (0.98). Before the *Event*,  
530 we also observed the highest values of  $\delta^{15}\text{N}$  at approximately 13.3‰, which we previously interpreted  
531 as an influence of the emissions from domestic heating via coal and/or biomass burning. Positive  
532 correlations of  $\delta^{13}\text{C}$  with oxalate and potassium (both 0.93) and the negative correlation with  
533 temperature (-0.79) also suggest that the *Event* is associated with fresh emissions from burning sources.

534

535 In contrast, we find that most  $\delta^{15}\text{N}$  values with a depletion of  $^{15}\text{N}$  are associated with enhanced  $\text{NH}_4^+$   
536 contents (70-80 % of TN) and almost absence of  $\text{NO}_3^-$  nitrogen (see Figs. 3 and 4). Although some

537 content of OrgN is detected during the *Event* (Fig. 3), the correlation between  $\delta^{15}\text{N}$  and OrgN/TN is not  
538 significant (Table 2). This result suggests that nitrogen with the lowest  $\delta^{15}\text{N}$  values is mainly connected  
539 with  $\text{NH}_4^+$ , which is supported by a strong negative correlation between  $\delta^{15}\text{N}$  and  $\text{NH}_4^+/\text{TN}$  (-0.86).  
540 Assuming that nitrogen in particles mainly originates from gaseous nitrogen precursors via gas-to-  
541 particle conversion (e.g., Wang et al., 2017) during the *Event*, we could expect the nitrogen originated  
542 mainly from  $\text{NH}_3$  with depleted  $^{15}\text{N}$  but not nitrogen oxides. Agricultural emissions from both fertilizer  
543 application and animal waste are important sources of  $\text{NH}_3$  (Felix et al., 2013). Considering possible  
544 agriculture emission sources, there exist several collective farms, with both livestock (mainly cows,  
545 Holstein cattle) and crop production in the SE direction from the Košetice observatory – namely,  
546 Agropodnik Košetice (3.4 km away), Agrodam Hořepník (6.8 km) and Agrorev Červená Řečice (9.5  
547 km). Skippytyé et al. (2016) reported lower  $\delta^{15}\text{N}$  values of TN (+1 to +6‰) for agriculture-derived  
548 particulate matter of poultry farms, which are close to our values obtained during the *Event* (Fig. 9).

549  
550 The  $\delta^{15}\text{N}$  values from the *Event* are associated with an average temperature of below  $0^\circ\text{C}$  (Figs. 7 and  
551 9). Savard et al. (2017) observed the lowest values of  $\delta^{15}\text{N}$  of  $\text{NH}_3$  with temperatures below  $-5^\circ\text{C}$ , and  
552 the  $\text{NH}_4^+$  particles that were simultaneously sampled were also isotopically lighter compared to the  
553 samples collected under higher temperature conditions. They interpreted the result as a preferential dry  
554 deposition of heavier isotopic  $^{15}\text{NH}_3$  species during the cold period, whereas lighter  $^{14}\text{NH}_3$  species  
555 preferentially remains in the atmosphere. However, cold weather can also lead to a decline of ammonia  
556 fluxes from aerosol water surfaces, soil, etc. (Roelle and Aneja, 2002), which generally result in a deficit  
557 of ammonia in the atmosphere. Emissions from farms are not as limited by low temperature and are  
558 thus a main source of ammonia in this deficiency state. The removal of  $\text{NH}_3$  leads to a non-equilibrium  
559 state between the gas and aerosol phases. Such an absence of equilibrium exchange of  $\text{NH}_3$  between the  
560 gas and liquid/solid phases is considered to cause the  $\text{NH}_4^+/\text{SO}_4^{2-}$  molar ratios below 2 for the three  
561 most  $^{15}\text{N}$  depleted samples (Fig. 8). However, under such conditions, nitrate partitioning in PM is  
562 negligible. It should be mentioned, that a deficiency of ammonia in atmosphere during the winter *Event*  
563 leads to completely opposite  $\delta^{15}\text{N}$  values than in summer (see section 3.3) even if molar ratios  
564  $\text{NH}_4^+/\text{SO}_4^{2-}$  are below 2 in both cases.

565  
566 Unidirectional reactions of isotopically lighter  $\text{NH}_3$  with  $\text{H}_2\text{SO}_4$  in the atmosphere are strongly preferred  
567 by the kinetic isotope effect, which is, after several minutes, followed by enrichment of  $^{14}\text{NH}_3$  due to  
568 the newly established equilibrium (Heaton et al., 1997). Based on laboratory experiments, Heaton et al.  
569 (1997) estimated the isotopic enrichment factor between gas  $\text{NH}_3$  and particle  $\text{NH}_4^+$ ,  $\epsilon_{\text{NH}_4-\text{NH}_3}$ , to be  
570 +33‰. Savard et al. (2017) reported an isotopic difference ( $\Delta\delta^{15}\text{N}$ ) between  $\text{NH}_3$  (g) and particulate  
571  $\text{NH}_4^+$  as a function of temperature, whereas  $\Delta\delta^{15}\text{N}$  for a temperature of approximately  $0^\circ\text{C}$  was  
572 approximately 40‰. In both cases, after subtraction of these values (33 or 40‰) from the  $\delta^{15}\text{N}$  values  
573 of the measured *Event*, we obtain values from approximately -40 to -28‰, which are in a range of  $\delta^{15}\text{N}$ -

574  $\text{NH}_3$  (g) measured for agricultural emissions. These values are especially in good agreement with  $\delta^{15}\text{N}$   
575 of  $\text{NH}_3$  derived from cow waste (ca. -38 to -22‰, Felix et al., 2013).

576

577 Thus, during the course of the winter *Event*, we probably observed PM representing a mixture of  
578 aerosols from household heating characterized by higher amounts of  $\text{NO}_3^-$  and low value (8.2‰) of  
579  $\delta^{15}\text{N}$  of TN, which are gradually replaced by  $^{15}\text{N}$ -depleted agricultural aerosols. The whole process  
580 occurred under low temperature conditions that was first initiated by a deficiency of  $\text{NH}_3$  followed by  
581 an unidirectional (kinetic) reaction of isotopically lighter  $\text{NH}_3(\text{g}) \rightarrow \text{NH}_4^+(\text{p})$ , in which  $\text{NH}_3$  is mainly  
582 originated from agricultural sources SE of the Košetice station.

583

584 If the four lowest values of  $\delta^{15}\text{N}$  mainly represent agricultural aerosols, then it can be suggested that the  
585  $\delta^{13}\text{C}$  values from the same samples should originate from same sources. During the winter *Event*., the  
586  $\delta^{13}\text{C}$  values ranging from -26.2 to -25.4‰ belong to the most  $^{13}\text{C}$  enriched fine aerosols at the Košetice  
587 site. However, similar  $\delta^{13}\text{C}$  values were reported by Widory (2006) for particles from coal combustion  
588 (-25.6 to -24.6‰). Skipitytè et al. (2016) reported a mean value of  $\delta^{13}\text{C}$  of TC (-23.7±1.3‰) for PM1  
589 particles collected on a poultry farm, and suggested the litter as a possible source for the particles. Thus,  
590 in the case of  $\delta^{13}\text{C}$  values that we observed during the winter *Event* are probably caused by emissions  
591 from domestic heating than from agricultural sources. This is also supported by increased emissions of  
592  $\text{SO}_2$  from coal combustion to formation of sulfates.

#### 593 **4. Summary and Conclusions**

594

595 Based on the analysis of year-round data of stable carbon and nitrogen isotopes, we extracted important  
596 information on the processes taking place in fine aerosols during different seasons at the Central  
597 European station of Košetice. Seasonal variations were observed for  $\delta^{13}\text{C}$  and  $\delta^{15}\text{N}$ , as well as for TC  
598 and TN concentrations. The supporting data (i.e., ions, EC/OC, meteorology, trace gases) revealed  
599 characteristic processes that led to changes in the isotopic compositions on the site.

600 The main and gradual changes in nitrogen isotopic composition occurred in spring. During early spring,  
601 domestic heating with wood stoves is still common, with high nitrate concentrations in aerosols, which  
602 decreased toward the end of spring. Additionally, the temperature slowly increases and the overall  
603 situation leads to thermodynamic equilibrium exchange between gas ( $\text{NO}_x\text{-NH}_3\text{-SO}_2$  mixture) and  
604 aerosol ( $\text{NO}_3^-\text{-NH}_4^+\text{-SO}_4^{2-}$  mixture) phases, which causes an enrichment of  $^{15}\text{N}$  in aerosols. Enrichment  
605 of  $^{15}\text{N}$  ( $\Delta\delta^{15}\text{N}$ ) from the beginning to the end of spring was approximately +10‰. Gradual springtime  
606 changes in isotopic composition were also observed for  $\delta^{13}\text{C}$ , but the depletion was small, and  $\Delta\delta^{13}\text{C}$   
607 was only -1.4‰.

608

609 In summer, we observed the lowest concentrations of TC and TN; however, there was an enhanced  
610 enrichment of  $^{15}\text{N}$ , which was probably caused by the aging of nitrogenous aerosols, where ammonium  
611 sulfate and bisulfate is subjected to isotopic fractionation via equilibrium exchange between  $\text{NH}_3(\text{g})$   
612 and  $\text{NH}_4^+(\text{p})$  when  $\text{NH}_4^+/\text{SO}_4^{2-}$  molar ratio was less than 2. However, summer values of  $\delta^{15}\text{N}$  were still  
613 among the highest compared with those in previous studies, which can be explained by several factors.  
614 First, a fine aerosol fraction (PM1) is more reactive, and its residence time in the atmosphere is longer  
615 than coarse mode particles, leading to  $^{15}\text{N}$  enrichment in aged aerosols. Second, summer aerosols,  
616 compared to other seasons, contain a negligible amount of nitrate, contributing to a decrease in the  
617 average value of  $\delta^{15}\text{N}$  of TN. Although the summer  $\delta^{15}\text{N}$  values were the highest further  $^{15}\text{N}$  enrichment  
618 was minimized at this season. On the other hand, we observed an enrichment of  $^{13}\text{C}$  only in summer,  
619 which can be explained by the photooxidation processes of organics and is supported by the positive  
620 correlation of  $\delta^{13}\text{C}$  with temperature and ozone. Despite this slow enrichment process, summertime  
621  $\delta^{13}\text{C}$  values were the lowest compared to those in other seasons and referred predominantly to organic  
622 aerosols of biogenic origin.

623

624 In winter, we found the highest concentrations of TC and TN. Lower winter  $\delta^{15}\text{N}$  values were apparently  
625 influenced by fresh aerosols from combustion, which were strongly driven by the amount of nitrates  
626 (mainly  $\text{NH}_4\text{NO}_3$  in PM1), and led to an average winter value ( $13.3 \pm 0.7\%$ ) of  $\delta^{15}\text{N}$  of TN. Winter  $\delta^{13}\text{C}$   
627 values were more enriched than summer values, which are involved with the emissions from biomass  
628 and coal burning for domestic heating.

629

630 We observed an aerosol event in winter, which was characterized by low temperatures below the  
631 freezing point, stable southeast winds, and a unique isotope signature with a depletion of  $^{15}\text{N}$  and  
632 enrichment of  $^{13}\text{C}$ . The winter *Event* characterized by  $^{15}\text{N}$  depletion was probably caused by preferential  
633 unidirectional reactions between isotopically light ammonia, originated mainly from agriculture  
634 emissions, and sulfuric acid, resulting in  $(\text{NH}_4)_2\text{SO}_4$  and  $\text{NH}_4\text{HSO}_4$ . This process was probably  
635 supported by long-term cold weather leading to a deficiency of ammonia in the atmosphere (due to dry  
636 deposition and/or low fluxes), and subsequent suppression of nitrate to partitioning in aerosol.

637 The majority of yearly data showed a strong correlation between  $\delta^{15}\text{N}$  and ambient temperature,  
638 demonstrating an enrichment of  $^{15}\text{N}$  via isotopic equilibrium exchange between the gas and particulate  
639 phases. This process seemed to be one of the main mechanisms for  $^{15}\text{N}$  enrichment at the Košetice site,  
640 especially during spring. The most  $^{15}\text{N}$ -enriched summer and most  $^{15}\text{N}$ -depleted winter samples were  
641 limited for the partitioning of nitrate between gas and aerosols.

642

643 This study revealed a picture of the seasonal cycle of  $\delta^{15}\text{N}$  in aerosol TN at the Košetice site. The  
644 seasonal  $\delta^{13}\text{C}$  cycle was not so pronounced because they mainly depend on the isotopic composition of  
645 primary sources, which often overlapped. Although photochemical secondary oxidation reactions are

646 driven by the kinetic isotopic effect, the phase transfer probably did not play a crucial role in the case  
647 of carbon at the Central European site.

648

#### 649 **Author contributions:**

650 All authors contributed to the final version of this article. PV analyzed isotopes, total carbon and  
651 nitrogen, EC/OC, evaluated data and wrote the paper under the supervision of KK. JS was responsible  
652 for gravimetric results as well as ions and EC/OC measurements and contributed to the text revision.  
653 BK prepared samples for isotope analyses. VZ managed field campaign and provided advice and  
654 feedback throughout the drafting and submission process.

655

#### 656 **Acknowledgements**

657

658 This study was supported by funding from the Japan Society for the Promotion of Science (JSPS)  
659 through Grant-in-Aid No. 24221001, from the Ministry of Education, Youth and Sports of the Czech  
660 Republic under the project no. LM2015037 and under the grant ACTRIS-CZ RI  
661 (CZ.02.1.01/0.0/0.0/16\_013/0001315). We also thank the Czech Hydrometeorological Institute for  
662 providing its meteorological data and Dr. Milan Váňa and his colleagues from the Košetice Observatory  
663 for their valuable cooperation during the collection of samples. We appreciate the financial support of  
664 the JSPS fellowship to P. Vodička (P16760).

665

#### 666 **References:**

667

668 Aggarwal, S. G., Kawamura, K., Umarji, G. S., Tachibana, E., Patil, R. S. and Gupta, P. K.: Organic  
669 and inorganic markers and stable C-, N-isotopic compositions of tropical coastal aerosols from  
670 megacity Mumbai: Sources of organic aerosols and atmospheric processing, *Atmos. Chem. Phys.*,  
671 13(9), 4667–4680, doi:10.5194/acp-13-4667-2013, 2013.

672 Agnihotri, R., Mandal, T. K., Karapurkar, S. G., Naja, M., Gadi, R., Ahammed, Y. N., Kumar, A.,  
673 Saud, T. and Saxena, M.: Stable carbon and nitrogen isotopic composition of bulk aerosols over India  
674 and northern Indian Ocean, *Atmos. Environ.*, 45(17), 2828–2835,  
675 doi:10.1016/j.atmosenv.2011.03.003, 2011.

676 Ancelet, T., Davy, P. K., Trompeter, W. J., Markwitz, A. and Weatherburn, D. C.: Carbonaceous  
677 aerosols in an urban tunnel, *Atmos. Environ.*, 45(26), 4463–4469,  
678 doi:10.1016/j.atmosenv.2011.05.032, 2011.

679 Beyn, F., Matthias, V., Aulinger, A. and Dähnke, K.: Do N-isotopes in atmospheric nitrate deposition  
680 reflect air pollution levels?, *Atmos. Environ.*, 107, 281–288, doi:10.1016/j.atmosenv.2015.02.057,  
681 2015.

682 Bikkina, S., Kawamura, K. and Sarin, M.: Stable carbon and nitrogen isotopic composition of fine  
683 mode aerosols (PM<sub>2.5</sub>) over the Bay of Bengal: impact of continental sources, *Tellus B Chem. Phys.*  
684 *Meteorol.*, 68(1), 31518, doi:10.3402/tellusb.v68.31518, 2016.

685 Boreddy, S. K. R., Parvin, F., Kawamura, K., Zhu, C. and Lee, C. Te: Stable carbon and nitrogen  
686 isotopic compositions of fine aerosols (PM<sub>2.5</sub>) during an intensive biomass burning over Southeast

- 687 Asia: Influence of SOA and aging, *Atmos. Environ.*, 191(August), 478–489,  
688 doi:10.1016/j.atmosenv.2018.08.034, 2018.
- 689 Cachier, H.: Isotopic characterization of carbonaceous aerosols, *Aerosol Sci. Technol.*, 10(2), 379–  
690 385, doi:10.1080/02786828908959276, 1989.
- 691 Cavalli, F., Viana, M., Yttri, K. E., Genberg, J. and Putaud, J.-P.: Toward a standardised thermal-  
692 optical protocol for measuring atmospheric organic and elemental carbon: the EUSAAR protocol,  
693 *Atmos. Meas. Tech.*, 3(1), 79–89, doi:10.5194/amt-3-79-2010, 2010.
- 694 Ceburnis, D., Masalaite, A., Ovadnevaite, J., Garbaras, A., Remeikis, V., Maenhaut, W., Claeys, M.,  
695 Sciare, J., Baisnée, D. and O’Dowd, C. D.: Stable isotopes measurements reveal dual carbon pools  
696 contributing to organic matter enrichment in marine aerosol, *Sci. Rep.*, 6(July), 1–6,  
697 doi:10.1038/srep36675, 2016.
- 698 Cieżka, M., Modelska, M., Górka, M., Trojanowska-Olichwer, A. and Widory, D.: Chemical and  
699 isotopic interpretation of major ion compositions from precipitation: A one-year temporal monitoring  
700 study in Wrocław, SW Poland, *J. Atmos. Chem.*, 73, 61–80, doi:10.1007/s10874-015-9316-2, 2016.
- 701 Dean, J. R., Leng, M. J. and Mackay, A. W.: Is there an isotopic signature of the Anthropocene?,  
702 *Anthr. Rev.*, 1(3), 276–287, doi:10.1177/2053019614541631, 2014.
- 703 Felix, D. J., Elliott, E. M., Gish, T. J., McConnell, L. L. and Shaw, S. L.: Characterizing the isotopic  
704 composition of atmospheric ammonia emission sources using passive samplers and a combined  
705 oxidation-bacterial denitrifier approach, *Rapid Commun. Mass Spectrom.*, 27(20), 2239–2246,  
706 doi:10.1002/rcm.6679, 2013.
- 707 Felix, J. D., Elliott, E. M. and Shaw, S. L.: Nitrogen isotopic composition of coal-fired power plant  
708 NO<sub>x</sub>: Influence of emission controls and implications for global emission inventories, *Environ. Sci.*  
709 *Technol.*, 46(6), 3528–3535, doi:10.1021/es203355v, 2012.
- 710 Fisseha, R., Saurer, M., Jäggi, M., Siegwolf, R. T. W., Dommen, J., Szidat, S., Samburova, V. and  
711 Baltensperger, U.: Determination of primary and secondary sources of organic acids and  
712 carbonaceous aerosols using stable carbon isotopes, *Atmos. Environ.*, 43(2), 431–437,  
713 doi:10.1016/j.atmosenv.2008.08.041, 2009a.
- 714 Fisseha, R., Spahn, H., Wegener, R., Hohaus, T., Brasse, G., Wissel, H., Tillmann, R., Wahner, A.,  
715 Koppmann, R. and Kiendler-Scharr, A.: Stable carbon isotope composition of secondary organic  
716 aerosol from  $\beta$ -pinene oxidation, *J. Geophys. Res.*, 114(D2), D02304, doi:10.1029/2008JD011326,  
717 2009b.
- 718 Freyer, H. D.: Seasonal variation of <sup>15</sup>N/<sup>14</sup>N ratios in atmospheric nitrate species, *Tellus B*, 43(1),  
719 30–44, doi:10.1034/j.1600-0889.1991.00003.x, 1991.
- 720 Freyer, H. D., Kley, D., Volz-Thomas, A. and Kobel, K.: On the interaction of isotopic exchange  
721 processes with photochemical reactions in atmospheric oxides of nitrogen, *J. Geophys. Res.*, 98(D8),  
722 14791–14796, doi:10.1029/93JD00874, 1993.
- 723 Fuzzi, S., Baltensperger, U., Carslaw, K., Decesari, S., Denier Van Der Gon, H., Facchini, M. C.,  
724 Fowler, D., Koren, I., Langford, B., Lohmann, U., Nemitz, E., Pandis, S., Riipinen, I., Rudich, Y.,  
725 Schaap, M., Slowik, J. G., Spracklen, D. V., Vignati, E., Wild, M., Williams, M. and Gilardoni, S.:  
726 Particulate matter, air quality and climate: Lessons learned and future needs, *Atmos. Chem. Phys.*,  
727 15(14), 8217–8299, doi:10.5194/acp-15-8217-2015, 2015.
- 728 Gensch, I., Kiendler-Scharr, A. and Rudolph, J.: Isotope ratio studies of atmospheric organic  
729 compounds: Principles, methods, applications and potential, *Int. J. Mass Spectrom.*, 365–366, 206–  
730 221, doi:10.1016/j.ijms.2014.02.004, 2014.
- 731 Górka, M., Rybicki, M., Simoneit, B. R. T. and Marynowski, L.: Determination of multiple organic  
732 matter sources in aerosol PM<sub>10</sub> from Wrocław, Poland using molecular and stable carbon isotope

- 733 compositions, *Atmos. Environ.*, 89, 739–748, doi:10.1016/j.atmosenv.2014.02.064, 2014.
- 734 Harrison, R. M. and Pio, C. A.: Size-differentiated composition of inorganic atmospheric aerosols of  
735 both marine and polluted continental origin, *Atmos. Environ.*, 17(9), 1733–1738, doi:10.1016/0004-  
736 6981(83)90180-4, 1983.
- 737 Heaton, T. H. E.: 15N/14N ratios of NO<sub>x</sub> from vehicle engines and coal-fired power stations, *Tellus*  
738 B, 42, 304–307, 1990.
- 739 Heaton, T. H. E., Spiro, B. and Robertson, S. M. C.: Potential canopy influences on the isotopic  
740 composition of nitrogen and sulphur in atmospheric deposition, *Oecologia*, (109), 600–607, 1997.
- 741 Hyslop, N. P.: Impaired visibility: the air pollution people see, *Atmos. Environ.*, 43(1), 182–195,  
742 doi:10.1016/j.atmosenv.2008.09.067, 2009.
- 743 Irei, S., Huang, L., Collin, F., Zhang, W., Hastie, D. and Rudolph, J.: Flow reactor studies of the  
744 stable carbon isotope composition of secondary particulate organic matter generated by OH-radical-  
745 induced reactions of toluene, *Atmos. Environ.*, 40(30), 5858–5867,  
746 doi:10.1016/j.atmosenv.2006.05.001, 2006.
- 747 Jickells, T., Baker, A. R., Cape, J. N., Cornell, S. E. and Nemitz, E.: The cycling of organic nitrogen  
748 through the atmosphere., *Philos. Trans. R. Soc. Lond. B. Biol. Sci.*, 368(1621), 20130115,  
749 doi:10.1098/rstb.2013.0115, 2013.
- 750 Kawamura, K., Kobayashi, M., Tsubonuma, N., Mochida, M., Watanabe, T. and Lee, M.: Organic  
751 and inorganic compositions of marine aerosols from East Asia: Seasonal variations of water-soluble  
752 dicarboxylic acids, major ions, total carbon and nitrogen, and stable C and N isotopic composition,  
753 *Geochemical Soc. Spec. Publ.*, 9(C), 243–265, doi:10.1016/S1873-9881(04)80019-1, 2004.
- 754 Kawashima, H. and Haneishi, Y.: Effects of combustion emissions from the Eurasian continent in  
755 winter on seasonal  $\delta^{13}\text{C}$  of elemental carbon in aerosols in Japan, *Atmos. Environ.*, 46, 568–579,  
756 doi:10.1016/j.atmosenv.2011.05.015, 2012.
- 757 Kawashima, H. and Kurahashi, T.: Inorganic ion and nitrogen isotopic compositions of atmospheric  
758 aerosols at Yurihonjo, Japan: Implications for nitrogen sources, *Atmos. Environ.*, 45(35), 6309–6316,  
759 doi:10.1016/j.atmosenv.2011.08.057, 2011.
- 760 Kundu, S., Kawamura, K. and Lee, M.: Seasonal variation of the concentrations of nitrogenous  
761 species and their nitrogen isotopic ratios in aerosols at Gosan, Jeju Island: Implications for  
762 atmospheric processing and source changes of aerosols, *J. Geophys. Res. Atmos.*, 115(20), 1–19,  
763 doi:10.1029/2009JD013323, 2010.
- 764 Kunwar, B., Kawamura, K. and Zhu, C.: Stable carbon and nitrogen isotopic compositions of ambient  
765 aerosols collected from Okinawa Island in the western North Pacific Rim, an outflow region of Asian  
766 dusts and pollutants, *Atmos. Environ.*, 131, 243–253, doi:10.1016/j.atmosenv.2016.01.035, 2016.
- 767 Li, D. and Wang, X.: Nitrogen isotopic signature of soil-released nitric oxide (NO) after fertilizer  
768 application, *Atmos. Environ.*, 42(19), 4747–4754, doi:10.1016/j.atmosenv.2008.01.042, 2008.
- 769 Liggio, J., Li, S. M., Vlasenko, A., Stroud, C. and Makar, P.: Depression of ammonia uptake to  
770 sulfuric acid aerosols by competing uptake of ambient organic gases, *Environ. Sci. Technol.*, 45(7),  
771 2790–2796, doi:10.1021/es103801g, 2011.
- 772 Martinelli, L. A., Camargo, P. B., Lara, L. B. L. S., Victoria, R. L. and Artaxo, P.: Stable carbon and  
773 nitrogen isotopic composition of bulk aerosol particles in a C<sub>4</sub> plant landscape of southeast Brazil,  
774 *Atmos. Environ.*, 36(14), 2427–2432, doi:10.1016/S1352-2310(01)00454-X, 2002.
- 775 Martinsson, J., Andersson, A., Sporre, M. K., Friberg, J., Kristensson, A., Swietlicki, E., Olsson, P. A.  
776 and Stenström, K. E.: Evaluation of  $\delta^{13}\text{C}$  in carbonaceous aerosol source apportionment at a rural  
777 measurement site, *Aerosol Air Qual. Res.*, 17, 2081–2094, doi:10.4209/aaqr.2016.09.0392, 2017.

778 Masalaite, A., Remeikis, V., Garbaras, A., Dudoitis, V., Ulevicius, V. and Ceburnis, D.: Elucidating  
779 carbonaceous aerosol sources by the stable carbon  $\delta^{13}C_{TC}$  ratio in size-segregated particles, *Atmos.*  
780 *Res.*, 158–159, 1–12, doi:10.1016/j.atmosres.2015.01.014, 2015.

781 Masalaite, A., Holzinger, R., Remeikis, V., Röckmann, T. and Dusek, U.: Characteristics, sources and  
782 evolution of fine aerosol (PM<sub>1</sub>) at urban, coastal and forest background sites in Lithuania, *Atmos.*  
783 *Environ.*, 148, 62–76, doi:10.1016/j.atmosenv.2016.10.038, 2017.

784 Mbengue, S., Fusek, M., Schwarz, J., Vodička, P., Šmejkalová, A. H. and Holoubek, I.: Four years of  
785 highly time resolved measurements of elemental and organic carbon at a rural background site in  
786 Central Europe, *Atmos. Environ.*, 182, 335–346, doi:10.1016/j.atmosenv.2018.03.056, 2018.

787 Meier-Augenstein, W. and Kemp, H. F.: *Stable Isotope Analysis: General Principles and Limitations*,  
788 in *Wiley Encyclopedia of Forensic Science*, American Cancer Society., 2012.

789 Miyazaki, Y., Kawamura, K., Jung, J., Furutani, H. and Uematsu, M.: Latitudinal distributions of  
790 organic nitrogen and organic carbon in marine aerosols over the western North Pacific, *Atmos. Chem.*  
791 *Phys.*, 11(7), 3037–3049, doi:10.5194/acp-11-3037-2011, 2011.

792 Mkomu, S., Kawamura, K., Tachibana, E. and Fu, P.: Stable carbon and nitrogen isotopic  
793 compositions of tropical atmospheric aerosols: sources and contribution from burning of C<sub>3</sub> and C<sub>4</sub>  
794 plants to organic aerosols, *Tellus B*, 66, 20176, doi:10.3402/tellusb.v66.20176, 2014.

795 Morera-Gómez, Y., Santamaría, J. M., Elustondo, D., Alonso-Hernández, C. M. and Widory, D.:  
796 Carbon and nitrogen isotopes unravels sources of aerosol contamination at Caribbean rural and urban  
797 coastal sites, *Sci. Total Environ.*, 642, 723–732, doi:10.1016/j.scitotenv.2018.06.106, 2018.

798 Neff, J. C., Holland, E. A., Dentener, F. J., McDowell, W. H. and Russell, K. M.: The origin,  
799 composition and rates of organic nitrogen deposition: a missing piece of the nitrogen cycle?,  
800 *Biogeochemistry*, 57/58, 99–136, 2002.

801 Park, Y., Park, K., Kim, H., Yu, S., Noh, S., Kim, M., Kim, J., Ahn, J., Lee, M., Seok, K. and Kim,  
802 Y.: Characterizing isotopic compositions of TC-C, NO<sub>3</sub>-N, and NH<sub>4</sub><sup>+</sup>-N in PM<sub>2.5</sub> in South Korea:  
803 Impact of China's winter heating, *Environ. Pollut.*, 233, 735–744, doi:10.1016/j.envpol.2017.10.072,  
804 2018.

805 Pavuluri, C. M. and Kawamura, K.: Enrichment of <sup>13</sup>C in diacids and related compounds during  
806 photochemical processing of aqueous aerosols: New proxy for organic aerosols aging, *Sci. Rep.*,  
807 6(October), 36467, doi:10.1038/srep36467, 2016.

808 Pavuluri, C. M. and Kawamura, K.: Seasonal changes in TC and WSOC and their <sup>13</sup>C isotope ratios  
809 in Northeast Asian aerosols: land surface–biosphere–atmosphere interactions, *Acta Geochim.*, 36(3),  
810 355–358, doi:10.1007/s11631-017-0157-3, 2017.

811 Pavuluri, C. M., Kawamura, K., Tachibana, E. and Swaminathan, T.: Elevated nitrogen isotope ratios  
812 of tropical Indian aerosols from Chennai: Implication for the origins of aerosol nitrogen in South and  
813 Southeast Asia, *Atmos. Environ.*, 44(29), 3597–3604, doi:10.1016/j.atmosenv.2010.05.039, 2010.

814 Pavuluri, C. M., Kawamura, K. and Fu, P. Q.: Atmospheric chemistry of nitrogenous aerosols in  
815 northeastern Asia: Biological sources and secondary formation, *Atmos. Chem. Phys.*, 15(17), 9883–  
816 9896, doi:10.5194/acp-15-9883-2015, 2015a.

817 Pavuluri, C. M., Kawamura, K. and Swaminathan, T.: Time-resolved distributions of bulk parameters,  
818 diacids, ketoacids and  $\alpha$ -dicarbonyls and stable carbon and nitrogen isotope ratios of TC and TN in  
819 tropical Indian aerosols: Influence of land/sea breeze and secondary processes, *Atmos. Res.*, 153,  
820 188–199, doi:10.1016/j.atmosres.2014.08.011, 2015b.

821 Pichlmayer, F., Schöner, W., Seibert, P., Stichler, W. and Wagenbach, D.: Stable isotope analysis for  
822 characterization of pollutants at high elevation alpine sites, *Atmos. Environ.*, 32(23), 4075–4085,  
823 doi:10.1016/S1352-2310(97)00405-6, 1998.

- 824 Pokorná, P., Schwarz, J., Krejci, R., Swietlicki, E., Havránek, V. and Ždímal, V.: Comparison of  
825 PM<sub>2.5</sub> chemical composition and sources at a rural background site in Central Europe between  
826 1993/1994/1995 and 2009/2010: Effect of legislative regulations and economic transformation on the  
827 air quality, *Environ. Pollut.*, 241, 841–851, doi:10.1016/j.envpol.2018.06.015, 2018.
- 828 Rahn, T. and Eiler, J. M.: Experimental constraints on the fractionation of C-13/C-12 and O-18/O-16  
829 ratios due to adsorption of CO<sub>2</sub> on mineral substrates at conditions relevant to the surface of Mars,  
830 *Geochim. Cosmochim. Acta*, 65(5), 839–846, 2001.
- 831 Roelle, P. A. and Aneja, V. P.: Characterization of ammonia emissions from soils in the upper coastal  
832 plain, North Carolina, *Atmos. Environ.*, 36(6), 1087–1097, doi:10.1016/S1352-2310(01)00355-7,  
833 2002.
- 834 Savard, M. M., Cole, A., Smirnoff, A. and Vet, R.:  $\delta^{15}\text{N}$  values of atmospheric N species  
835 simultaneously collected using sector-based samplers distant from sources – Isotopic inheritance and  
836 fractionation, *Atmos. Environ.*, 162, 11–22, doi:10.1016/j.atmosenv.2017.05.010, 2017.
- 837 Schwarz, J., Cusack, M., Karban, J., Chalupníčková, E., Havránek, V., Smolík, J. and Ždímal, V.:  
838 PM<sub>2.5</sub> chemical composition at a rural background site in Central Europe, including correlation and  
839 air mass back trajectory analysis, *Atmos. Res.*, 176–177, 108–120,  
840 doi:10.1016/j.atmosres.2016.02.017, 2016.
- 841 Silvern, R. F., Jacob, D. J., Kim, P. S., Marais, E. A., Turner, J. R., Campuzano-Jost, P. and Jimenez,  
842 J. L.: Inconsistency of ammonium-sulfate aerosol ratios with thermodynamic models in the eastern  
843 US: A possible role of organic aerosol, *Atmos. Chem. Phys.*, 17(8), 5107–5118, doi:10.5194/acp-17-  
844 5107-2017, 2017.
- 845 Skipitytė, R., Mašalaitė, A., Garbaras, A., Mickienė, R., Ragažinskienė, O., Baliukonienė, V.,  
846 Bakutis, B., Šiugždaitė, J., Petkevičius, S., Maruška, A. S. and Remeikis, V.: Stable isotope ratio  
847 method for the characterisation of the poultry house environment, *Isotopes Environ. Health Stud.*,  
848 53(3), 243–260, doi:10.1080/10256016.2016.1230609, 2016.
- 849 Stein, A. F., Draxler, R. R., Rolph, G. D., Stunder, B. J. B., Cohen, M. D. and Ngan, F.: Noaa's  
850 hysplit atmospheric transport and dispersion modeling system, *Bull. Am. Meteorol. Soc.*, 96(12),  
851 2059–2077, doi:10.1175/BAMS-D-14-00110.1, 2015.
- 852 Stelson, A. W., Friedlander, S. K. and Seinfeld, J. H.: A note on the equilibrium relationship between  
853 ammonia and nitric acid and particulate ammonium nitrate, *Atmos. Environ.*, 13(3), 369–371,  
854 doi:10.1016/0004-6981(79)90293-2, 1979.
- 855 Ti, C., Gao, B., Luo, Y., Wang, X., Wang, S. and Yan, X.: Isotopic characterization of NH<sub>x</sub>-N in  
856 deposition and major emission sources, *Biogeochemistry*, 138(1), 85–102, doi:10.1007/s10533-018-  
857 0432-3, 2018.
- 858 Váňa, M. and Dvorská, A.: Košetice Observatory - 25 years, 1. edition., Czech Hydrometeorological  
859 Institute, Prague., 2014.
- 860 Vodička, P., Schwarz, J., Cusack, M. and Ždímal, V.: Detailed comparison of OC/EC aerosol at an  
861 urban and a rural Czech background site during summer and winter, *Sci. Total Environ.*, 518–519(2),  
862 424–433, doi:10.1016/j.scitotenv.2015.03.029, 2015.
- 863 Walters, W. W., Simonini, D. S. and Michalski, G.: Nitrogen isotope exchange between NO and NO  
864 2 and its implications for  $\delta^{15}\text{N}$  variations in tropospheric NO<sub>x</sub> and atmospheric nitrate, *Geophys.*  
865 *Res. Lett.*, (2), 1–26, doi:10.1002/2015GL066438, 2015a.
- 866 Walters, W. W., Goodwin, S. R. and Michalski, G.: Nitrogen stable isotope composition ( $\delta^{15}\text{N}$ ) of  
867 vehicle-emitted NO<sub>x</sub>, *Environ. Sci. Technol.*, 49(4), 2278–2285, doi:10.1021/es505580v, 2015b.
- 868 Wang, G., Xie, M., Hu, S., Gao, S., Tachibana, E. and Kawamura, K.: Dicarboxylic acids, metals and  
869 isotopic compositions of C and N in atmospheric aerosols from inland China: Implications for dust

870 and coal burning emission and secondary aerosol formation, *Atmos. Chem. Phys.*, 10(13), 6087–  
871 6096, doi:10.5194/acp-10-6087-2010, 2010.

872 Wang, Y. L., Liu, X. Y., Song, W., Yang, W., Han, B., Dou, X. Y., Zhao, X. D., Song, Z. L., Liu, C.  
873 Q. and Bai, Z. P.: Source appointment of nitrogen in PM<sub>2.5</sub> based on bulk  $\delta^{15}\text{N}$  signatures and a  
874 Bayesian isotope mixing model, *Tellus, Ser. B Chem. Phys. Meteorol.*, 69(1), 1–10,  
875 doi:10.1080/16000889.2017.1299672, 2017.

876 Weber, R. J., Guo, H., Russell, A. G. and Nenes, A.: High aerosol acidity despite declining  
877 atmospheric sulfate concentrations over the past 15 years, *Nat. Geosci.*, 9(4), 282–285,  
878 doi:10.1038/ngeo2665, 2016.

879 Widory, D.: Combustibles, fuels and their combustion products: A view through carbon isotopes,  
880 *Combust. Theory Model.*, 10(5), 831–841, doi:10.1080/13647830600720264, 2006.

881 Widory, D.: Nitrogen isotopes: Tracers of origin and processes affecting PM<sub>10</sub> in the atmosphere of  
882 Paris, *Atmos. Environ.*, 41(11), 2382–2390, doi:10.1016/j.atmosenv.2006.11.009, 2007.

883 Widory, D., Roy, S., Le Moullec, Y., Goupil, G., Cocherie, A. and Guerrot, C.: The origin of  
884 atmospheric particles in Paris: A view through carbon and lead isotopes, *Atmos. Environ.*, 38(7),  
885 953–961, doi:10.1016/j.atmosenv.2003.11.001, 2004.

886 Xiao, H.-W., Xiao, H.-Y., Luo, L., Zhang, Z.-Y., Huang, Q.-W., Sun, Q.-B. and Zeng, Z.: Stable  
887 carbon and nitrogen isotope compositions of bulk aerosol samples over the South China Sea, *Atmos.*  
888 *Environ.*, 193, 1–10, doi:https://doi.org/10.1016/j.atmosenv.2018.09.006, 2018.

889 Xue, D., Botte, J., Baets, B. De, Accoe, F., Nestler, A., Taylor, P., Cleemput, O. Van, Berglund, M.  
890 and Boeckx, P.: Present limitations and future prospects of stable isotope methods for nitrate source  
891 identification in surface- and groundwater, *Water Res.*, 43(5), 1159–1170,  
892 doi:https://doi.org/10.1016/j.watres.2008.12.048, 2009.

893 Yeatman, S. G., Spokes, L. J., Dennis, P. F. and Jickells, T. D.: Can the study of nitrogen isotopic  
894 composition in size-segregated aerosol nitrate and ammonium be used to investigate atmospheric  
895 processing mechanisms?, *Atmos. Environ.*, 35(7), 1337–1345, doi:10.1016/S1352-2310(00)00457-X,  
896 2001a.

897 Yeatman, S. G., Spokes, L. J., Dennis, P. F. and Jickells, T. D.: Comparisons of aerosol nitrogen  
898 isotopic composition at two polluted coastal sites, *Atmos. Environ.*, 35(7), 1307–1320,  
899 doi:10.1016/S1352-2310(00)00408-8, 2001b.

900 Zhang, Y. L., Kawamura, K., Cao, F. and Lee, M.: Stable carbon isotopic compositions of low-  
901 molecular-weight dicarboxylic acids, oxocarboxylic acids,  $\alpha$ -dicarbonyls, and fatty acids:  
902 Implications for atmospheric processing of organic aerosols, *J. Geophys. Res. Atmos.*, 121(7), 3707–  
903 3717, doi:10.1002/2015JD024081, 2016.

904 Zíková, N. and Ždímal, V.: Long-term measurement of aerosol number size distributions at rural  
905 background station Košetice, *Aerosol Air Qual. Res.*, 13(5), 1464–1474,  
906 doi:10.4209/aaqr.2013.02.0056, 2013.

907

908

909

910 Table 1: Seasonal and entire campaign averages  $\pm$  standard deviations, (medians in brackets) of  
 911 different variables.

	<b>Autumn</b>	<b>Winter</b>	<b>Spring</b>	<b>Summer</b>	<b>Year</b>
<b>N of samples</b>	25	45	43	33	146
<b>TC [<math>\mu\text{g m}^{-3}</math>] (from EA)</b>	3.61 $\pm$ 1.61 (3.30)	4.76 $\pm$ 2.44 (3.88)	3.78 $\pm$ 2.03 (3.04)	2.71 $\pm$ 0.76 (2.68)	3.81 $\pm$ 2.03 (3.35)
<b>TN [<math>\mu\text{g m}^{-3}</math>]</b>	1.56 $\pm$ 1.18 (1.33)	1.67 $\pm$ 0.96 (1.45)	2.00 $\pm$ 1.62 (1.47)	0.81 $\pm$ 0.29 (0.82)	1.56 $\pm$ 1.22 (1.26)
<b><math>\delta^{13}\text{C}</math> [‰]</b>	-26.8 $\pm$ 0.5 (-26.9)	-26.7 $\pm$ 0.5 (-26.7)	-27.1 $\pm$ 0.5 (-27.0)	-27.8 $\pm$ 0.4 (-27.7)	-27.1 $\pm$ 0.6 (-27.0)
<b><math>\delta^{15}\text{N}</math> [‰]</b>	17.1 $\pm$ 2.4 (16.9)	13.1 $\pm$ 4.5 (15.2)	17.6 $\pm$ 3.5 (17.3)	25.0 $\pm$ 1.6 (25.1)	17.8 $\pm$ 5.5 (16.9)
<b>TC/PM1 [%]</b>	28 $\pm$ 6 (26)	33 $\pm$ 8 (32)	38 $\pm$ 15 (35)	31 $\pm$ 6 (30)	33 $\pm$ 11 (31)
<b>TN/PM1 [%]</b>	11 $\pm$ 3 (11)	11 $\pm$ 3 (12)	17 $\pm$ 4 (17)	9 $\pm$ 2 (9)	12 $\pm$ 4 (12)
<b>NO<sub>3</sub><sup>-</sup>-N/TN [%]</b>	21 $\pm$ 6 (21)	25 $\pm$ 8 (28)	22 $\pm$ 8 (21)	5 $\pm$ 3 (4)	19 $\pm$ 10 (20)
<b>NH<sub>4</sub><sup>+</sup>-N/TN [%]</b>	51 $\pm$ 6 (51)	51 $\pm$ 9 (49)	58 $\pm$ 7 (60)	57 $\pm$ 6 (57)	54 $\pm$ 8 (54)
<b>OrgN/TN [%]</b>	28 $\pm$ 8 (26)	25 $\pm$ 8 (23)	20 $\pm$ 8 (19)	39 $\pm$ 6 (38)	27 $\pm$ 10 (25)
<b>TC/TN</b>	2.77 $\pm$ 1.10 (2.60)	3.34 $\pm$ 1.66 (2.68)	2.33 $\pm$ 0.98 (2.34)	3.60 $\pm$ 1.23 (3.45)	3.01 $\pm$ 1.38 (2.61)

912

913 Table 2: Spearman correlation coefficients (r) of  $\delta^{15}\text{N}$  with various tracers. Only bold values are  
 914 statistically significant (p-values < 0.05).

<b><math>\delta^{15}\text{N}</math> vs.</b>	<b>Autumn</b>	<b>Winter*</b>	<b>Spring</b>	<b>Summer</b>	<b>Year*</b>	<b>Event</b>
<b>TN</b>	-0.30	<b>-0.40</b>	<b>-0.70</b>	<b>0.36</b>	<b>-0.54</b>	<b>0.93</b>
<b>TN/PM1</b>	<b>-0.63</b>	<b>-0.50</b>	-0.02	<b>0.37</b>	<b>-0.35</b>	0.36
<b>NO<sub>3</sub><sup>-</sup>-N/TN</b>	-0.39	-0.04	<b>-0.73</b>	-0.26	<b>-0.77</b>	<b>0.98</b>
<b>NH<sub>4</sub><sup>+</sup>-N/TN</b>	0.16	-0.30	<b>0.60</b>	<b>0.52</b>	<b>0.42</b>	<b>-0.86</b>
<b>OrgN/TN</b>	0.20	<b>0.38</b>	0.20	-0.33	<b>0.51</b>	-0.71
<b>NO<sub>3</sub><sup>-</sup></b>	<b>-0.41</b>	<b>-0.35</b>	<b>-0.80</b>	-0.03	<b>-0.78</b>	<b>0.96</b>
<b>NH<sub>4</sub><sup>+</sup></b>	-0.22	<b>-0.42</b>	<b>-0.61</b>	<b>0.40</b>	<b>-0.44</b>	0.75
<b>OrgN</b>	-0.26	-0.27	<b>-0.56</b>	0.30	<b>-0.25</b>	0.71
<b>SO<sub>4</sub><sup>2-</sup></b>	-0.07	<b>-0.38</b>	-0.30	<b>0.51</b>	0.03	-0.57
<b>Cl</b>	-0.37	-0.18	<b>-0.74</b>	<b>-0.37</b>	<b>-0.74</b>	<b>0.99</b>
<b>O<sub>3</sub> (gas)</b>	<b>0.45</b>	0.14	0.15	-0.02	<b>0.40</b>	-0.71
<b>NO<sub>2</sub> (gas)</b>	<b>-0.53</b>	<b>-0.34</b>	<b>-0.72</b>	0.20	<b>-0.64</b>	<b>0.86</b>
<b>NO<sub>2</sub>/NO (gas)</b>	<b>-0.51</b>	-0.26	<b>-0.82</b>	0.14	<b>-0.76</b>	<b>0.82</b>
<b>Temp.</b>	<b>0.58</b>	0.30	<b>0.52</b>	-0.21	<b>0.77</b>	-0.43

915 \*Event data are excluded from winter and year datasets.

916

917

918

919

920

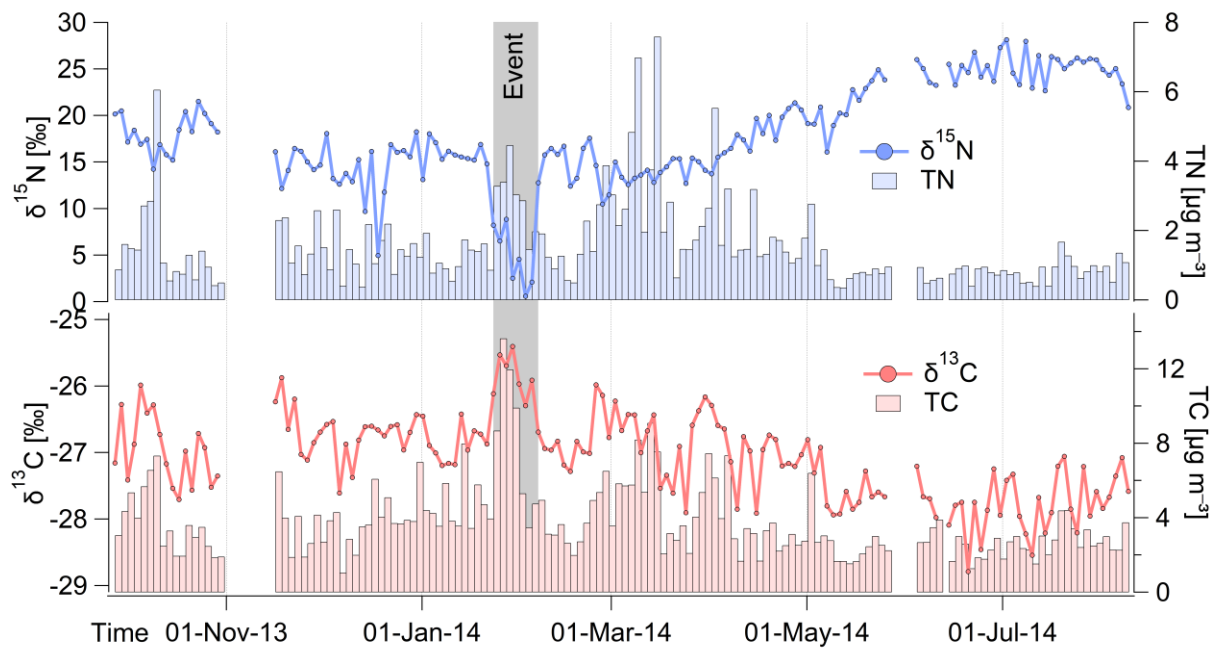
921 Table 3: Spearman correlation coefficients ( $r$ ) of  $\delta^{13}\text{C}$  with various tracers. Only bold values are  
 922 statistically significant (p-values < 0.05).

$\delta^{13}\text{C}$ vs.	Autumn	Winter*	Spring	Summer	Year*	Event
<b>OC</b>	<b>0.64</b>	<b>0.63</b>	<b>0.91</b>	<b>0.39</b>	<b>0.75</b>	0.75
<b>EC</b>	<b>0.61</b>	<b>0.74</b>	<b>0.88</b>	0.28	<b>0.84</b>	0.46
<b>EC/TC</b>	0.06	0.06	0.13	<b>-0.51</b>	<b>0.32</b>	-0.32
<b>TC/PM1</b>	-0.16	-0.05	<b>-0.40</b>	0.22	-0.09	0.32
<b>NO<sub>3</sub><sup>-</sup></b>	<b>0.74</b>	<b>0.52</b>	<b>0.71</b>	0.12	<b>0.76</b>	0.39
<b>NH<sub>4</sub><sup>+</sup></b>	<b>0.84</b>	<b>0.59</b>	<b>0.80</b>	<b>0.42</b>	<b>0.66</b>	0.75
<b>Oxalate</b>	0.34	<b>0.62</b>	<b>0.71</b>	<b>0.65</b>	<b>0.25</b>	<b>0.93</b>
<b>SO<sub>4</sub><sup>2-</sup></b>	<b>0.80</b>	<b>0.64</b>	<b>0.73</b>	<b>0.41</b>	<b>0.34</b>	0.54
<b>K<sup>+</sup></b>	<b>0.84</b>	<b>0.63</b>	<b>0.70</b>	<b>0.47</b>	<b>0.76</b>	<b>0.93</b>
<b>Cl<sup>-</sup></b>	<b>0.44</b>	<b>0.62</b>	<b>0.68</b>	<b>0.44</b>	<b>0.76</b>	0.25
<b>CO (gas)</b>	0.21	<b>0.53</b>	<b>0.60</b>	0.32	<b>0.37</b>	0.68
<b>O<sub>3</sub> (gas)</b>	<b>-0.41</b>	-0.26	0.14	<b>0.66</b>	<b>-0.33</b>	0.11
<b>NO<sub>2</sub> (gas)</b>	<b>0.67</b>	<b>0.38</b>	<b>0.70</b>	0.18	<b>0.69</b>	0.32
<b>NO<sub>2</sub>/NO (gas)</b>	<b>0.72</b>	<b>0.65</b>	<b>0.67</b>	<b>0.68</b>	<b>0.78</b>	<b>0.96</b>
<b>Temp.</b>	-0.33	<b>-0.35</b>	-0.20	<b>0.39</b>	<b>-0.57</b>	<b>-0.79</b>

923 \*Event data are excluded from winter and year datasets.

924

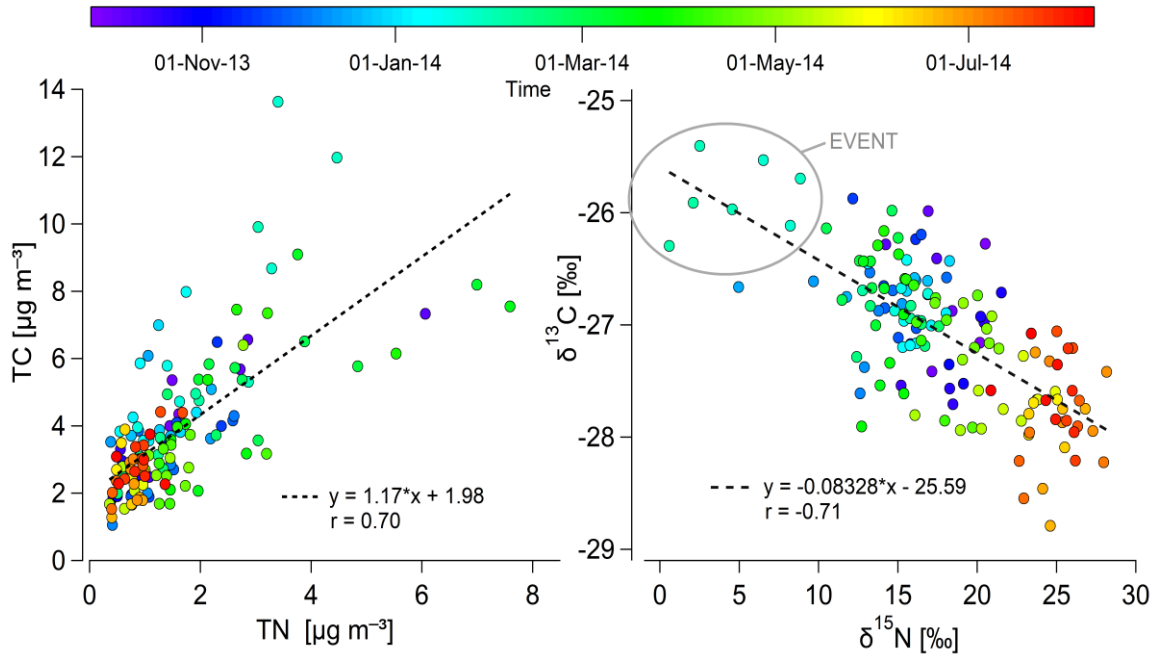
925



926

927

928 Fig. 1: Time series of  $\delta^{15}\text{N}$  along with TN (top) and  $\delta^{13}\text{C}$  as well as TC (bottom) in PM1 aerosols at the  
 929 Košice station. The gray color highlights an *Event* with divergent values, especially for  $\delta^{15}\text{N}$ .

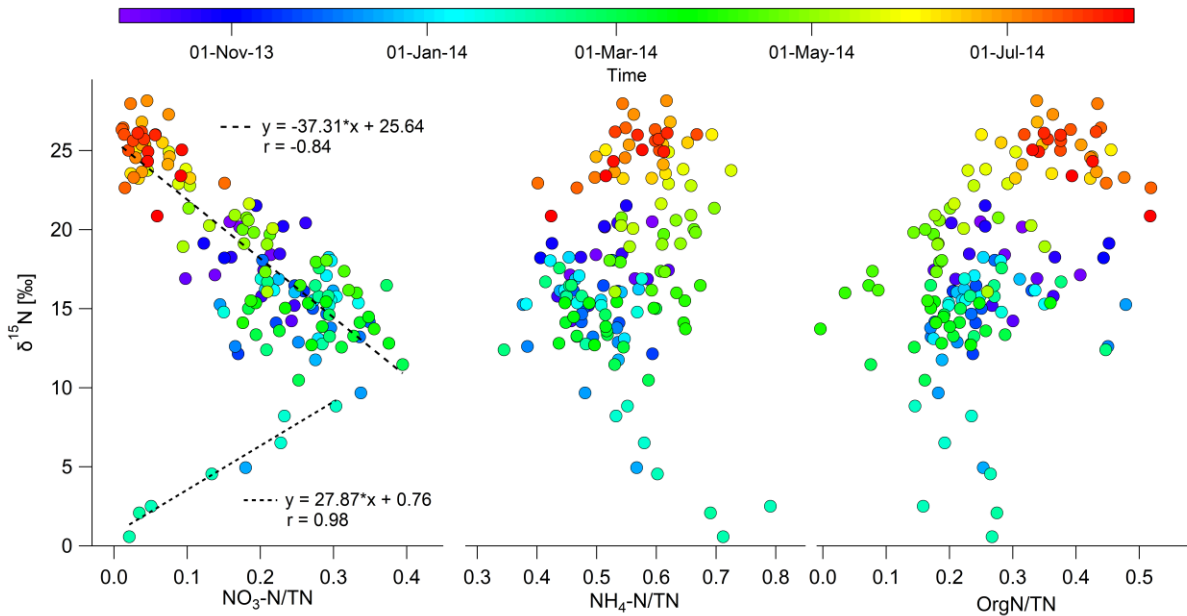


930

931 Fig. 2: Relationships between TC and TN (left) and their stable carbon and nitrogen isotopes (right).  
 932 The color scale reflects the time of sample collection. The gray circle highlights the winter *Event*  
 933 measurements.

934

935

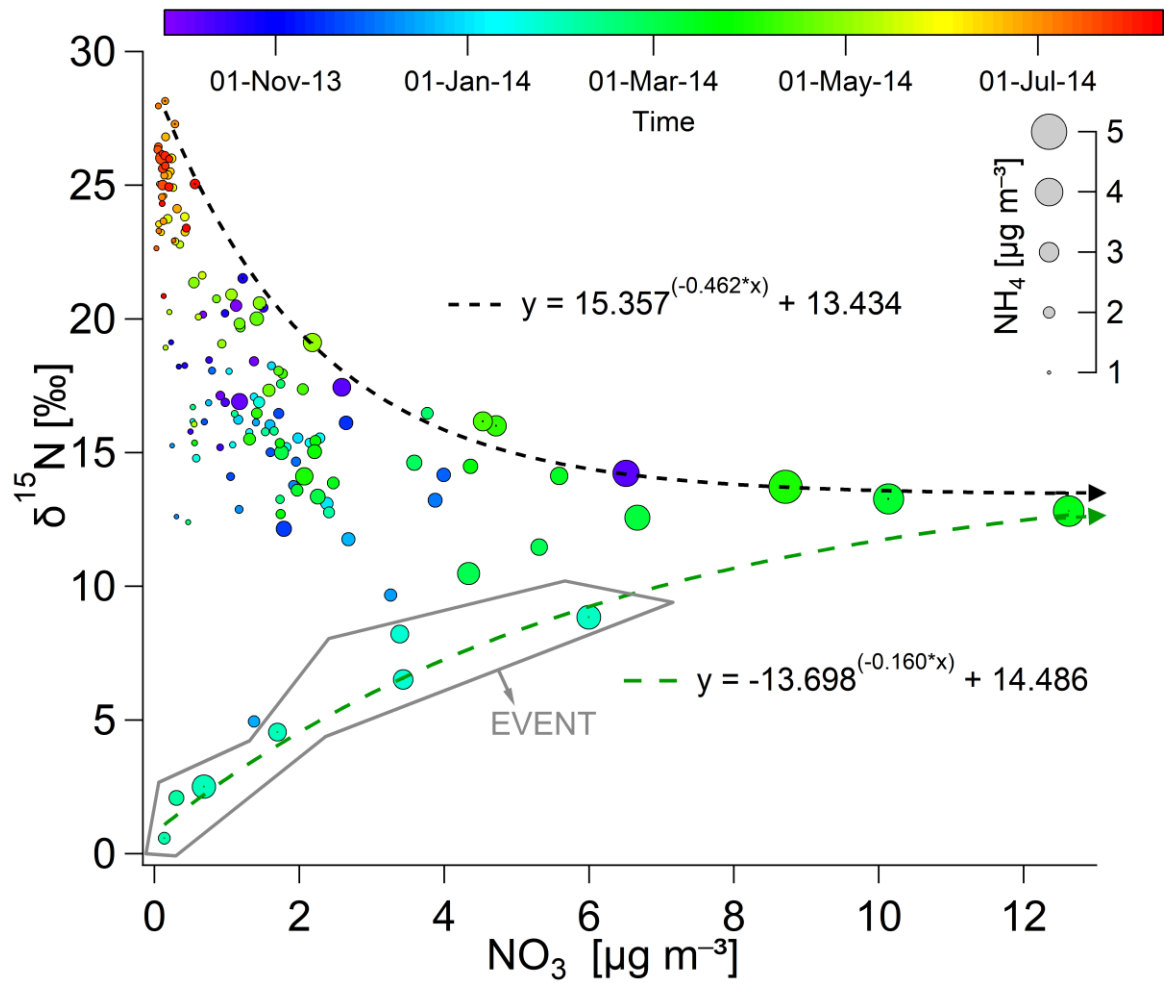


936

937

938 Fig. 3: Changes in  $\delta^{15}\text{N}$  depending on fraction of individual nitrogen components ( $\text{NO}_3\text{-N}$ ,  $\text{NH}_4\text{-N}$ , and  
 939  $\text{OrgN}$ ) in TN. The color scale reflects the time of sample collection.

940

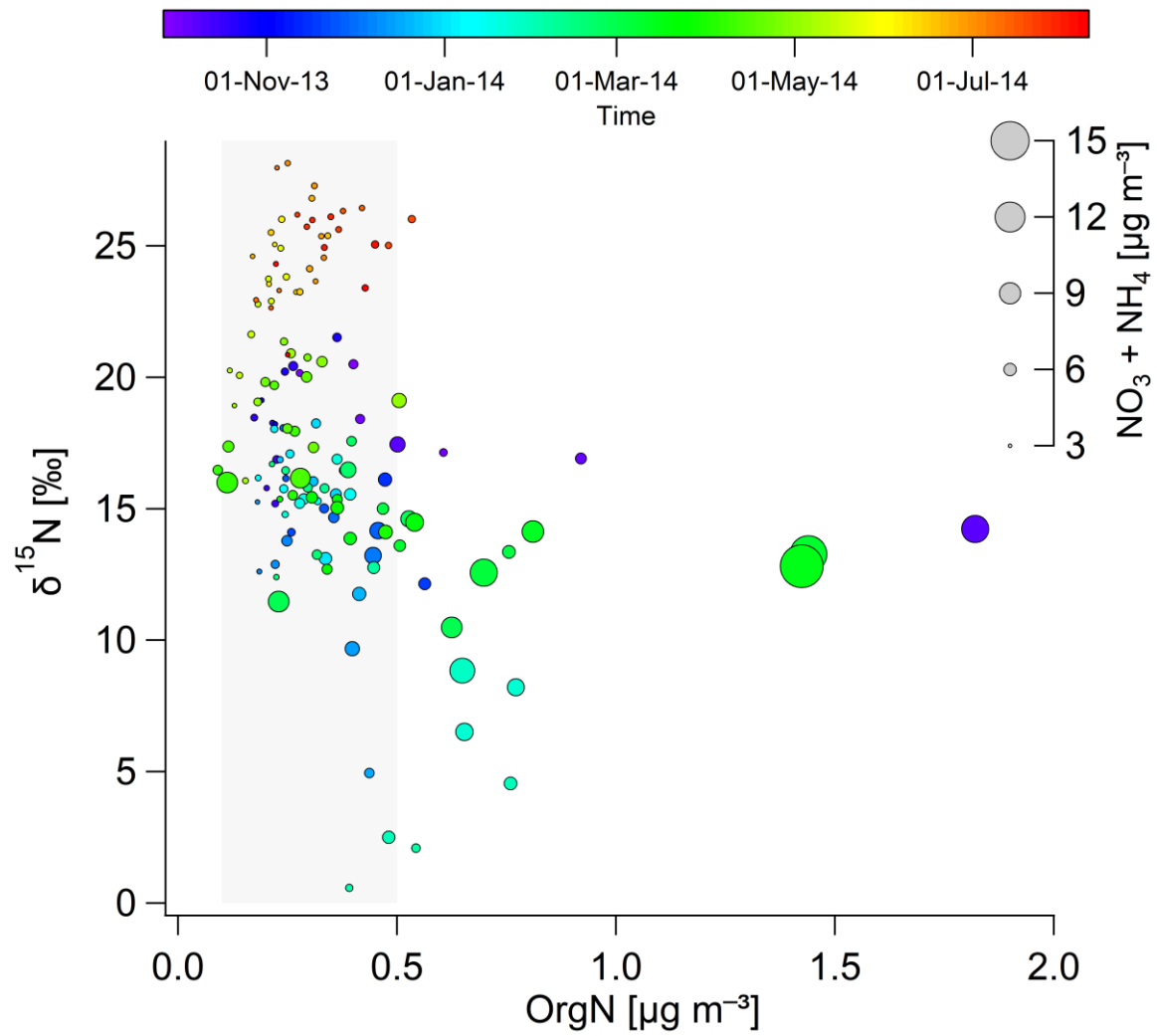


941

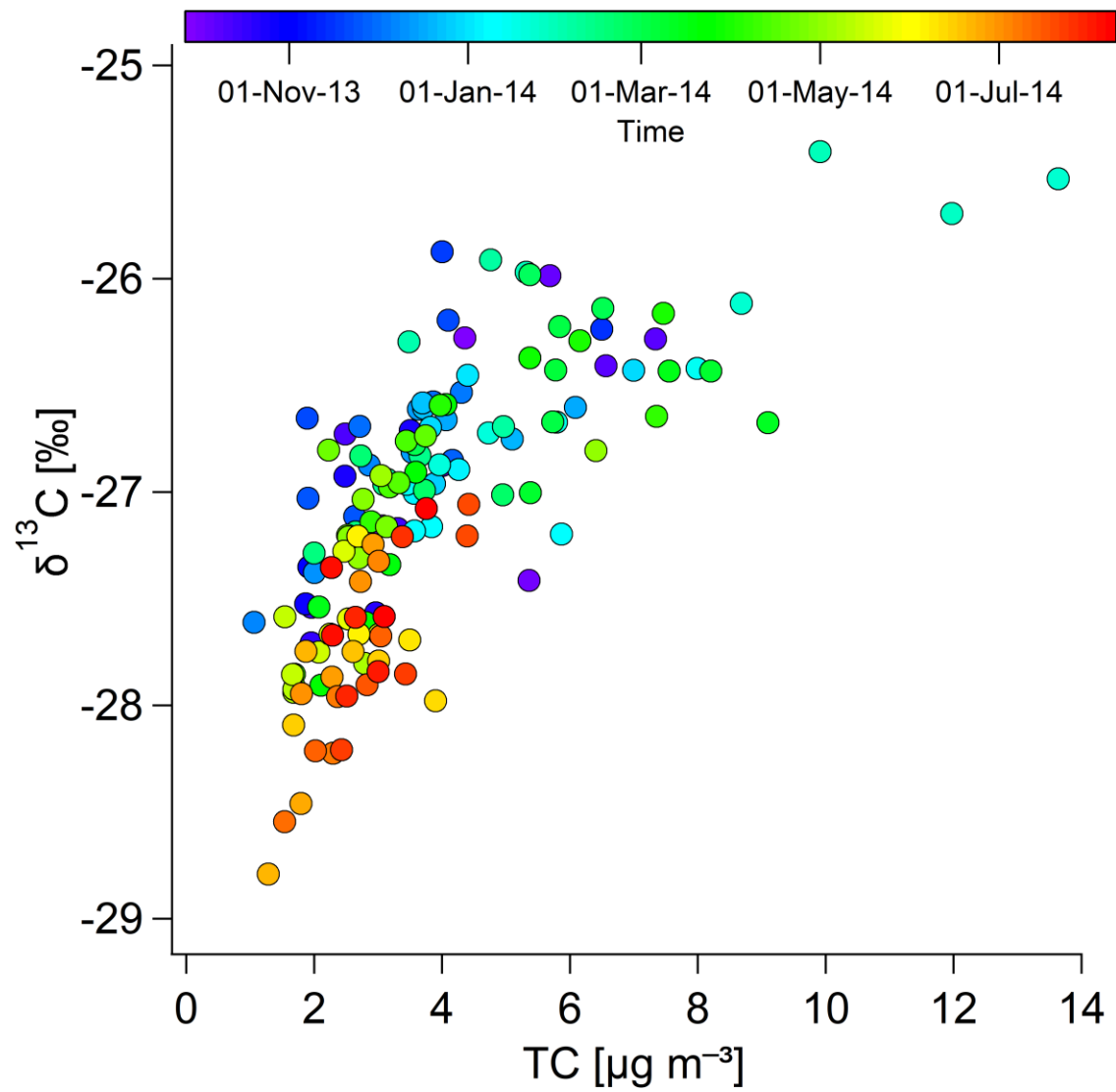
942 Fig. 4: Relationships of δ<sup>15</sup>N of TN vs. NO<sub>3</sub><sup>-</sup> concentrations. The larger circles indicate higher NH<sub>4</sub><sup>+</sup>  
 943 concentrations. The color scale reflects the time of sample collection.

944

945

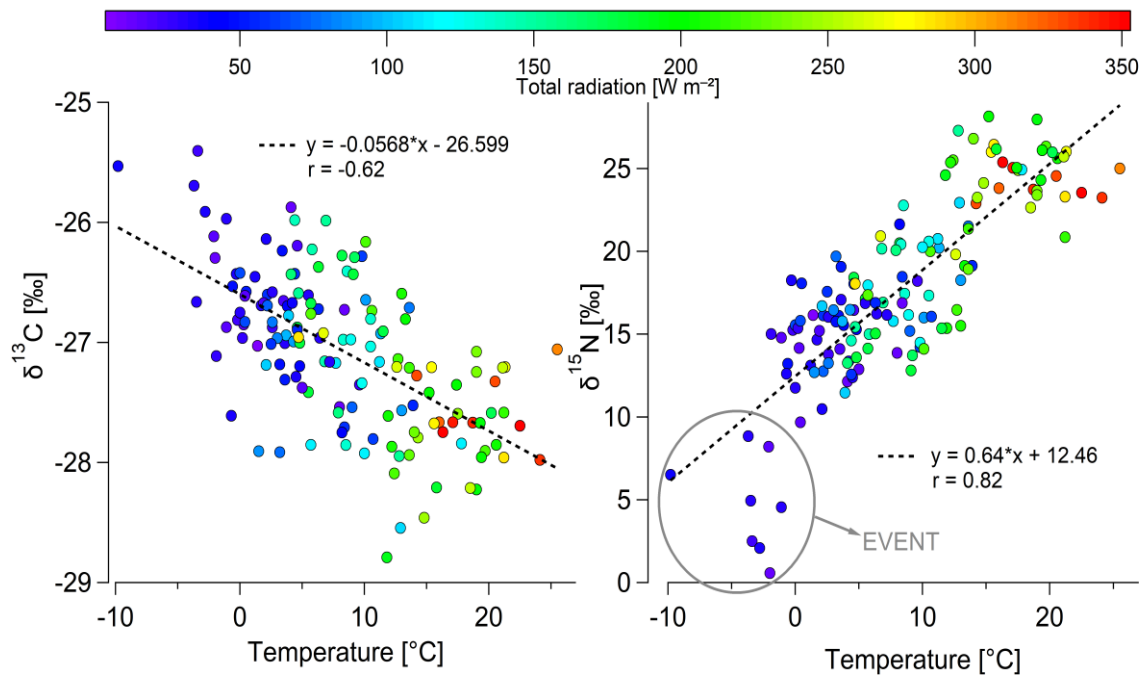


946  
 947 Fig. 5: Relationships of  $\delta^{15}\text{N}$  of TN vs. OrgN concentrations. The larger circles indicate higher sums of  
 948  $\text{NO}_3^- + \text{NH}_4^+$  concentrations. The color scale reflects the time of sample collection, and the highlighted  
 949 portion is a concentration range between 0.1-0.5  $\mu\text{g m}^{-3}$ .



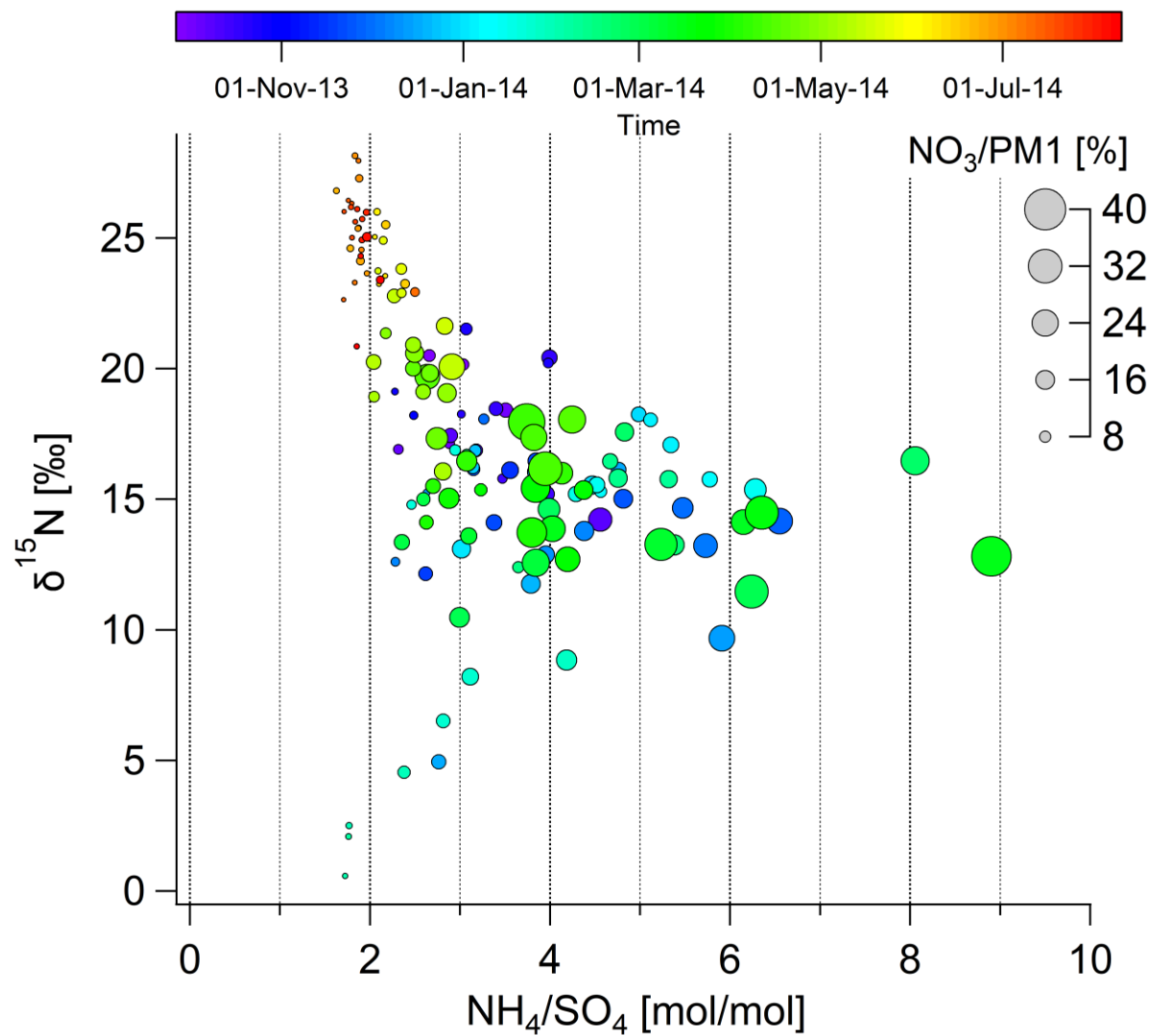
950  
 951  
 952

Fig. 6: Relationship between TC and  $\delta^{13}\text{C}$ . The color scale reflects the time of sample collection.



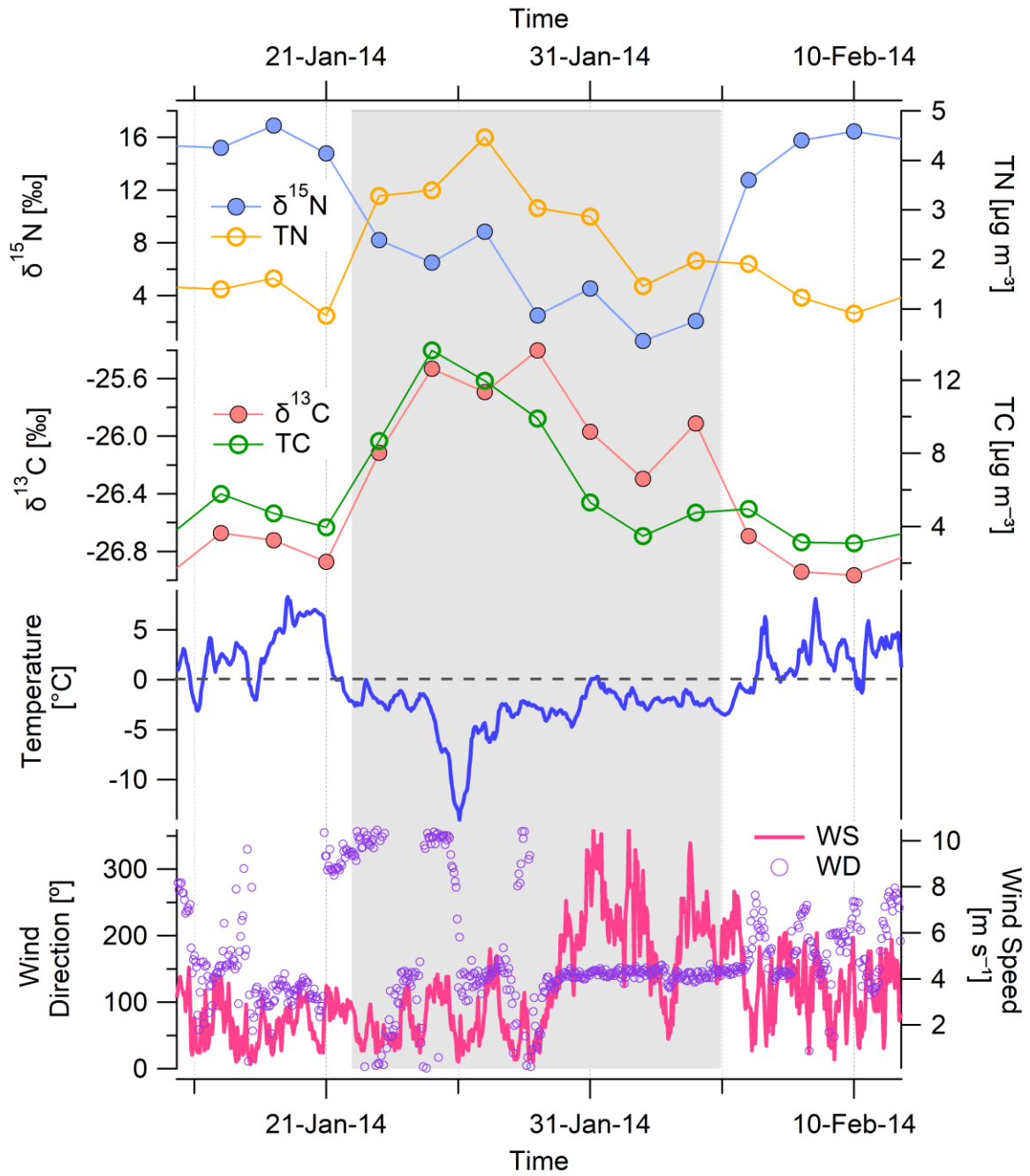
953

954 Fig. 7: Relationships between temperature and  $\delta^{13}\text{C}$  of TC (left) and  $\delta^{15}\text{N}$  of TN (right). The color scale  
 955 reflects the total radiation.



956

957 Fig. 8: Relationships between  $\delta^{15}\text{N}$  of TN and molar ratios of  $\text{NH}_4^+/\text{SO}_4^{2-}$  in particles. The larger circle  
 958 indicates higher nitrate content in PM1. The color scale reflects the time of sample collection.



959  
 960 Fig. 9: Time series of  $\delta^{15}\text{N}$ , TN,  $\delta^{13}\text{C}$ , TC and meteorological variables (temperature, wind speed and  
 961 direction, 1 h time resolution) during the *Event*, which is highlighted by the gray color.  
 962

